INTERNATIONAL JOURNAL FOR NUMERICAL METHODS IN FLUIDS
Int. J. Numer. Meth. Fluids 2010; **00**:1–35
Published online in Wiley InterScience (www.interscience.wiley.com). DOI: 10.1002/fld

An enthalpy-preserving shock-capturing term for Residual Distribution Schemes

J. Garicano-Mena[1,*] and G. Degrez[2]

[1] *ETSIAE-UPM (School of Aeronautics), Plaza Cardenal Cisneros 3, E-28040 Madrid, España*
[2] *Service Aéro-Thermo-Mécanique, Université Libre de Bruxelles, Avenue F. D. Roosevelt 50, Bruxelles, 1050, Belgique*

SUMMARY

In this contribution we investigate strategies to perform shock capturing computation of steady hypersonic flow fields by means of residual distribution schemes. The ultimate objective is the computation of flow solutions for which the correct upstream enthalpy value is recovered in the post-shock region.
To this end, the parallelism existing between the classical Bx scheme and stabilized finite element techniques is exploited. The simple Lax-Friedrichs dissipation term is leveraged to build two new residual distribution schemes. Upon testing on both inviscid and viscous steady problems, solutions obtained with one of the two schemes are shown to recover the correct upstream total enthalpy level in the post-shock region.
This last scheme provides also improved wall pressure and skin friction predictions; heat transfer predictions are, unfortunately, similar to those offered by the Bx scheme. A conjecture for explaining this behavior is exposed.

Received . . .

KEY WORDS: Hypersonic flow; Adiabatic perfect gas; Residual distribution schemes; Shock capturing; Unstructured grids

1. INTRODUCTION

Most common strategies employed to solve numerically the scalar convection-diffusion equation resort to supplementing the *centrally* discretized gradient operators with properly designed *stabilization* [1]. In some cases, this stabilization can be identified as an independent term, whereas in other cases it is embedded into how gradients or fluxes are computed; in any case the stabilization introduces *artificial* dissipation that helps to prevent the appearance of unphysical oscillations in the numerical solution. Quite often, the artificial dissipation has a marked *upwind*-biased character [1, 2].

Artificial dissipation as that mentioned above is capable of stabilizing the computation provided there are no features characterized by strong, localized gradients, *i.e., shock fronts*. In those

*Correspondence to: J. Garicano-Mena, E-mail: jesus.garicano.mena@upm.es

occasions, one possible strategy [3] is to introduce yet another dissipative term, locally active with the aim of diffusing somewhat the discontinuous feature till it can be resolved on the underlying grid. These strategies are termed *shock-capturing* methods. Alternatively, approaches that consider shock fronts as pure discontinuities are termed *shock-fitting* methods (see [4] for a recent account on the topic).

The quite general paradigm of supplementing the centered discretization with an upwind-flavored stabilization term (and possibly an additional *shock-capturing* term where needed) lies at the root of different well-established numerical techniques. Moreover, the aforementioned principle applies as well to systems of advection-diffusion equations, e.g. the compressible Navier-Stokes equations. Indeed, many different numerical techniques exploiting this principle have been proposed in the literature: one can find numerical methods based on finite difference (*FD*) [5, 6], finite volume (*FV*) [7, 8, 9], streamline upwind Petrov-Galerkin finite element (*FE*) [10, 11, 12] and discontinuous Galerkin (*DG*) [13, 14] discretization.

A common concern for all the techniques so far referenced is the optimization of the stabilization terms employed. Indeed, one would desire to employ dissipative terms that avoid as effectively as possible unphysical oscillations in the computed solution. At the same time, one would prefer stabilization techniques to be such that any relevant features present in the solution, like shock fronts or boundary layers, are described as accurately as possible.

In this sense, numerical methods designers have to reconcile two major -and somewhat contradictory- constrains: *robustness* and *accuracy*. Solutions that involve stabilization and/or shock-capturing terms that respect as closely as possible the underlying physics of the problem at hand (*i.e.,* schemes that respect propagation of information along characteristics, enforce entropy increase and/or respect enthalpy preservation where adequate) are typically the most successful.

Focusing specifically on shock-capturing strategies, the early work in [15, 16] led Kitamura and his coauthors [8, 9] to identify the use of total-enthalpy preserving *FV* flux-functions as a desirable property when simulating hypersonic flow fields. Almost simultaneously, Kirk described a total-enthalpy preserving shock-capturing term in the context of stabilized *FE* methods [12]; Persson and Darmofal and his collaborators reached similar conclusions for *DG* methods, see [17, 14].

This contribution is concerned with shock-capturing residual distribution methods[18, 19]. Our goal is to devise a total-enthalpy preserving shock capturing term that can be employed in combination with residual distribution techniques.

Residual Distribution (or *RD*) [†] methods are vertex-centered discretization techniques capable of handling hyperbolic systems of equations on general unstructured simplicial grids. *RD* methods have been employed successfully for the discretization and solution of advection-diffusion scalar

[†] *RD* techniques sometimes referred as Fluctuation Splitting (*FS*) schemes[20].

DOI: 10.1002/fld

equations in [21, 22, 23, 24]; and for the compressible Navier-Stokes equations in the context of transonic aerodynamics in references [19, 25, 26, 27]. . . . In the hypersonic field, the method has been applied to double cone configurations [28, 29] and blunt body problems, both in shock-capturing ([30, 31, 32]) and shock fitting ([33, 34, 35, 36]) contexts.

The article is organized as follows: section 2 describes the system of equations that governs the non-reacting hypersonic flow fields of our interest. Next, section 3 introduces the Residual Distribution technique employed in this work. This section focuses mainly in the treatment of the advective contribution, and -by exploiting connections between stabilized *FE* and *RD* schemes- describes a strategy to build an enthalpy-preserving shock capturing term. The performance of the improved shock-capturing term is evaluated in section 4: the hypersonic, inviscid blunt body problem is employed as a benchmark, and special attention is paid to assess the robustness of the new scheme. The behavior of the new scheme when applied to hypersonic viscous problems is investigated in section 5. Finally, the conclusions of our study are summarized in section 6.

In an attempt to clarify as much as possible the discussion, all the necessary but non-essential material concerning e.g. details about handling viscous terms, enforcing boundary conditions and the solution procedure of the discrete system of nodal equations is gathered in appendix A.

2. GOVERNING EQUATIONS

The flow of a compressible, single-species, non-reacting gas is described by the following system of equations:

$$\begin{array}{lll} \dfrac{\partial \rho}{\partial t} & +\nabla\cdot(\rho\vec{u}) & = 0 \\ \dfrac{\partial \rho\vec{u}}{\partial t} & +\nabla\cdot\left(\rho\vec{u}\cdot\vec{u}^t + p\bar{\bar{I}}_{n_D}\right) & = \nabla\cdot\bar{\bar{\tau}}, \\ \dfrac{\partial \rho E}{\partial t} & +\nabla\cdot(\rho H\vec{u}) & = \nabla\cdot\left(\bar{\bar{\tau}}\cdot\vec{u} - \vec{q}\right), \end{array} \tag{1}$$

in the space-time domain $\Omega \times [0, T]$. In equation above, ρ stands for the gas density, and $\rho\vec{u}$ and ρE are the momentum and the total energy per unit volume, respectively. Additionally, p is the pressure exerted by the gas and H is the specific total enthalpy, which reads:

$$H = E + \frac{p}{\rho}. \tag{2}$$

The specific total energy E gathers both the specific internal energy e and the specific kinetic energy:

$$E = e + \frac{\|\vec{u}\|^2}{2}. \tag{3}$$

Prepared using fldauth.cls
DOI: 10.1002/fld

For the flow conditions considered in this work a perfect gas (PG) thermodynamic model is adequate. In that case the following relations hold:

$$p = R_g\,\rho\,T \text{ and } e = C_v\,T. \tag{4}$$

The gas constant R_g depends on the molecular weight of the gas under consideration. For air ($M_{air} = 28.84 kg/kmol$), $R_{air} = 288.29 J/K\,kg$; the specific heat capacity at constant volume C_v, which is constant for a calorically and thermally perfect gas, is given by $C_v = \frac{R_g}{\gamma - 1}$ with $\gamma = 1.4$ (air being considered a mixture of diatomic molecules). Sound speed is given by $a^2 = \gamma\,R_g\,T$.

Viscous stress tensor components $\tau_{i,j}$ are given, under the hypothesis of negligible bulk viscosity effects, by:

$$\tau_{i,j} = \mu\left[\left(\frac{\partial u_j}{\partial x_i} + \frac{\partial u_i}{\partial x_j}\right) - \frac{2}{3}\frac{\partial u_j}{\partial x_j}\right], \tag{5}$$

while heat flux components are defined as:

$$q_i = -\kappa\frac{\partial T}{\partial x_i}. \tag{6}$$

Regarding the transport properties in equations (5) and (6), the dynamic viscosity μ is given by the Sutherland law:

$$\mu = \mu_0\left(\frac{T}{T_0}\right)^{\frac{3}{2}}\frac{T_0 + C_s}{T + C_s}, \tag{7}$$

valid for moderate temperatures, $T \in (100\,K, 2000\,K)$. Typical values in this expression are $\mu_0 = 1.789 \times 10^{-5} kg/m\,s^2$, $T_0 = 288\,K$, and $C_s = 110\,K$, see [37]. The heat conductivity κ relates to viscosity under the assumption of constant Prandtl ($Pr = 0.71$ for air) number $\kappa = {}^{\mu\,C_p}/_{Pr}$. For an ideal gas, $C_p = C_v + R_g$.

System of equations (1) can be recast in compact, vector form as:

$$\frac{\partial \vec{U}}{\partial t} + \nabla\cdot\bar{\bar{F}}^c = \nabla\cdot\bar{\bar{F}}^d. \tag{8}$$

This reformulation eases the description of the numerical discretization of system (1) by means of Residual Distribution schemes, as we shall see in section 3. The vector of conserved variables $\vec{U}$ includes the density ρ, the momentum $\rho\vec{u}$ and the total ρE energy:

$$\vec{U} = [\rho, \quad \rho u_j, \quad \rho E]^t \in \mathbb{R}^{n_{Eqs}},\ n_{Eqs} = n_D + 2. \tag{9}$$

The components of the convective flux tensor are:

$$\vec{F}^c_j = [\rho\,u_j, \quad \rho\,u_i\,u_j + p\,\delta_{i,j}, \quad \rho\,H\,u_j]^t, \tag{10}$$

whereas the diffusive flux tensor is:

$$\vec{F}^d_j = [0, \quad \tau_{i,j}, \quad \tau_{i,j}\,u_j - q_i]^t. \tag{11}$$

DOI: 10.1002/fld

For the Residual Distribution discretization employed in this work it is useful to have this system of equations expressed in quasi-linear form, which is obtained by linearizing the advective flux tensor:

$$\frac{\partial \vec{U}}{\partial t} + \underbrace{\frac{\partial \vec{F}_j^c}{\partial \vec{U}}}_{A_j^{c,U}} \frac{\partial \vec{U}}{\partial x_j} = \frac{\partial \vec{F}_j^d}{\partial x_j}, \tag{12}$$

where we have introduced the advective Jacobians $A_j^{c,U} \in \mathbb{R}^{n_{Eqs} \times n_{Eqs}}$. For the *PG* model considered, the advective Jacobians are such that a matrix $\mathcal{A}$ defined as:

$$\mathcal{A} = A_j^{c,U} m_j, \forall \vec{m} \in \mathbb{R}^{n_D}, \tag{13}$$

has exactly n_{Eqs} real eigenvalues and n_{Eqs} linearly independent eigenvectors. That is equivalent to say that the associated advective system of equations, $\frac{\partial \vec{U}}{\partial t} + \nabla \cdot \bar{\bar{F}}^c = \vec{0}$ (see also Eq. (16)), is hyperbolic [2]. The eigenvalues of $\mathcal{A}$ are:

$$\vec{\lambda}_t = \left[\vec{u} \cdot \vec{m} + a, \underbrace{\vec{u} \cdot \vec{m}, \ldots, \vec{u} \cdot \vec{m}}_{n_D}, \vec{u} \cdot \vec{m} - a \right]^t, \tag{14}$$

Defining the diagonal matrix $\Lambda_t \equiv diag\left(\vec{\lambda}\right)$ and arranging the right/left eigenvectors as columns/rows in matrices R_t^U / L_t^U, $\mathcal{A}$ is factored as:

$$\mathcal{A} = R_m^U \cdot \Lambda_t \cdot L_m^U. \tag{15}$$

A large body of the results presented in this contribution concern inviscid flows. System of Eqs. 1 can be reduced to the one describing the behavior of an inviscid flow by simply disregarding contributions from the molecular processes (*i.e.,* assuming $\mu \to 0$ and $\kappa \to 0$), or equivalently disregarding the diffusive term tensor $\bar{\bar{F}}^d$. In that case, Eq. 1 boils down to:

$$\frac{\partial \vec{U}}{\partial t} + \nabla \cdot \bar{\bar{F}}^c = \vec{0}. \tag{16}$$

Finally, consider flows around an object immersed in a stream originating at a spatial region such that *upstream* flow properties are uniform. In that case, if the flow can be considered inviscid and a steady state solution is reached, then total enthalpy remains constant along streamlines, $\rho \vec{u} \cdot \nabla H = 0$, and the energy conservation equation is precisely the mass conservation equation scaled by the upstream total enthalpy H_∞, *i.e.,* :

$$H_\infty \nabla \cdot (\rho \vec{u}) = 0. \tag{17}$$

In section 3.3 we will discuss strategies to build shock-capturing schemes that preserve this relation between the mass and the total energy conservation equations at the discrete level.

DOI: 10.1002/fld

3. RESIDUAL DISTRIBUTION SCHEMES FOR THE NAVIER-STOKES EQUATIONS

Assume we intend to solve the system of equations (8) on a simplicial tessellation Ω^h of the spatial domain Ω. Let us denote by n_{Elem} and n_{DoF} the number of *simplices* (triangles in `2D` , tetrahedra in `3D`) and vertices in Ω^h. The numerical solution to Eq. (8), $\vec{U}^h$ [‡] can be immediately expanded in terms of the associated nodal basis functions $N_j \in P^1\left(\Omega^h\right)$, see Fig. 1a:

$$\vec{U}^h\left(\vec{x},t\right) = \sum_{j=1}^{n_{DoF}} \vec{U}_j\left(t\right) N_j\left(\vec{x}\right) \tag{18}$$

where the nodal basis functions N_j fulfill $N_j\left(\vec{x}_k\right) = \delta_{j,k}$.

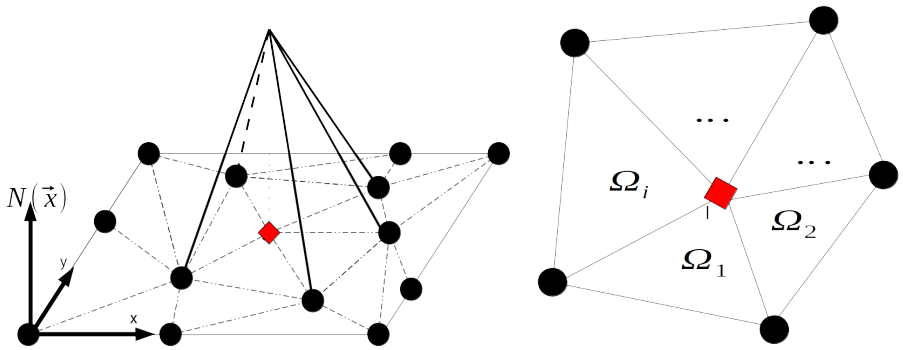

Figure 1. Discretization in *RDS* : (a), $P1$ nodal basis function for l-th node; (b), set Ξ_l of elements surrounding l-th node.

The steady state residual for element Ω_i *-i.e.,* the flux balance-is defined as:

$$\vec{\Phi}^{\Omega_i} = \int_{\Omega_i} \left(\frac{\partial \vec{F}_j^c}{\partial x_j} - \frac{\partial \vec{F}_j^d}{\partial x_j} \right) dv = \vec{\Phi}^{c,\Omega_i} - \vec{\Phi}^{d,\Omega_i}, \tag{19}$$

and gathers contributions from the convective and diffusive terms.

An equation for each of the nodal *DoF* 's is obtained by distributing fractions of the cell residuals $\vec{\Phi}^{\Omega_i}$ to the nodes forming part of the cell; in this manner, the l-th *DoF* collects contributions from all the elements forming region Ξ_l (see Fig. 1b):

$$\vec{\Phi}_l = \sum_{\Omega_i \in \Xi_l} \vec{\Phi}_l^{\Omega_i} = \sum_{\Omega_i \in \Xi_l} \left(\mathfrak{f}^c\left(\vec{\Phi}^{c,\Omega_i}\right) + \mathfrak{f}^d\left(\vec{\Phi}^{d,\Omega_i}\right) \right). \tag{20}$$

How the functionals $\mathfrak{f}^c, \mathfrak{f}^d$ in Eq. (20) are chosen defines the specific *RD* scheme employed. The rest of this section focuses on the computation and distribution of the convective residuals

[‡]Superscript h marks here the solution obtained as a numerical approximation. Unless we want to insist on this fact, we will often drop the superscript.

Prepared using fldauth.cls
DOI: 10.1002/fld

for shocked flows; handling the residual contributions from the diffusive term and the boundary conditions (*BC*), together with the solution strategy are deferred to Appendix A.

Specifically, we will describe in detail three established *RD* schemes, -namely, the N, LDA and the Bx schemes- dwelling on how they are related. This will allow to establish a link with stabilized *FE* techniques. This link will be the basis for the definition of new *RD* schemes, some of which have improved capabilities regarding total enthalpy preservation across strong detached shock waves.

3.1. Three classical RD schemes

We start by describing how the convective residual $\vec{\Phi}^{\Omega_i}$ is computed: the multi-dimensional extension [38] of the Roe linearization [5], allows to compute the elemental convective residual as:

$$\vec{\Phi}^{c,\Omega_i} = \sum_{k\in\Omega_i} K_k \vec{U}_k, \tag{21}$$

where K_k are the nodal upwind parameters, computed by:

$$K_k = \frac{1}{n_D} A^{c,U}_{x_d}\, n_{x_d,k}, \text{ and } k \in \{1,\dots,n_D+1\}. \tag{22}$$

These nodal upwind parameters are defined by the inward-pointing scaled nodal normals $\vec{n}_k$ (see Figure 2a) and the convective Jacobians $A^{c,U}_{x_d}$. These Jacobians need to be evaluated precisely at the state corresponding to the cell Roe average in order to discrete conservation to be guaranteed [38].

The element-to-node distribution is expressed in terms of the nodal upwind parameters K_k, usually by defining a distribution matrix $B^{\Omega_i}_k(K_k)$. The specific dependence of B_k on the upwind parameters determines the properties of the advective scheme [18].

Low diffusion A scheme

Introduced originally in [39], Van der Weide and collaborators derived the distribution matrix for system of equations in [40, 19]. The LDA element-to-node contribution is computed as the matrix-vector product $B^{\Omega_i,LDA}_l \cdot \vec{\Phi}^{c,\Omega_i}$, where the *distribution matrix* is given by:

$$B^{\Omega_i,LDA}_l = K^+_l \cdot \left(\sum_j K^+_j\right)^{-1}. \tag{23}$$

Operator $()^+$ simply sets to zero negative entries in Λ_t before pre and postmultiplying by R_l and L_l, see equation 15.

The LDA scheme is linear and is multidimensional upwind. Since the distribution matrices $B^{\Omega_i,LDA}_l$ are uniformly bounded, the LDA scheme is Linearity Preserving [18], *i.e.,* is 2^{nd} order accurate at steady state, (that it, it preserves linear solutions). It is widely used for the simulation of

DOI: 10.1002/fld

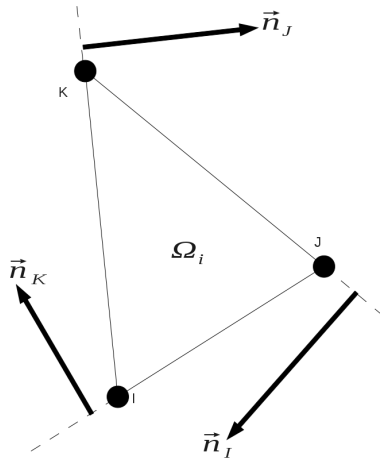

(a)

Figure 2. Discretization in *RDS* : inward-pointing scaled nodal normals for i-th element.

smooth flow fields [41, 42, 43, 35].

Narrow scheme

The scalar N was devised by Roe in [44], and reformulated as a matrix *RD* scheme by van der Weide in [45, 19]. The N scheme contribution to the nodal residual is given by:

$$\vec{\Phi}_l^{c,\Omega_i,N} = K_l^+ \cdot \left(\vec{U}_l - \vec{U}_{inlet}^{\Omega_i}\right). \tag{24}$$

where the *inlet* state $\vec{U}_{inlet}^{\Omega_i}$ reads:

$$\vec{U}_{inlet}^{\Omega_i} = \left(\sum_{j\in\Omega_i} K_j^-\right)^{-1} \cdot \sum_{j\in\Omega_i} K_j^- \cdot \vec{U}_j. \tag{25}$$

The N scheme is linear, multi-dimensional upwind and *positive*; hence it is only 1^{st} order accurate, in agreement with Godunov's theorem. Note that a distribution matrix cannot be obtained explicitly for the system N scheme.

There is an important relationship between the N and the LDA schemes, namely that N scheme is precisely the LDA scheme supplemented by an additional dissipative term $\vec{\delta}_l^{Diss,N}$ of crosswind nature [46, 47]:

$$\vec{\Phi}_l^{c,\Omega_i,N} = \vec{\Phi}_l^{c,\Omega_i,LDA} + \vec{\delta}_l^{Diss,N}. \tag{26}$$

DOI: 10.1002/fld

Blended schemes

A family of non-linear schemes can be obtained from a weighted averaging of N and LDA schemes:

$$\vec{\Phi}_l^{c,\Omega_i,B} = \Theta^{\Omega_i}\vec{\Phi}_l^{c,\Omega_i,N} + \left(\bar{\bar{I}}_{nEqs} - \Theta^{\Omega_i}\right)\vec{\Phi}_l^{c,\Omega_i,LDA}, \tag{27}$$

The resulting scheme is therefore multi-dimensional upwind, positive and linearity preserving. Many variants can be constructed [19, 18, 22, 42, 48, 24] depending on the choice of Θ^{Ω_i}. Here, we will use the shock detector function of Dobeš and Deconinck; this combination is known in the literature as Bx scheme. Matrix Θ^{Ω_i} is taken as the identity matrix times a scalar shock sensor θ (see [49]):

$$\Theta^{\Omega_i} = \theta\bar{\bar{I}}_{nEqs}. \tag{28}$$

The scalar shock sensor θ above depends on the gradient of one of the field variables (e.g. density, temperature or pressure), and requires tuning a parameter related to the shock intensity [49]. In the results presented in this work pressure has been used throughout as the sensing variable.

The shock sensor is defined in terms of the positive part of projection of the discrete gradient $\nabla^h p$ along the speed over the cell $\vec{u}^{\Omega_i}$, namely $\sigma = \left(\vec{u}^{\Omega_i}\cdot\nabla^h p\right)^+$. This projection is compared against the tunable *scale parameter* $S \equiv {}^{U\,\Delta P}/_{L}$. The complete expression is:

$$\theta^{\Omega_i} = \min\left(h\left(\frac{\sigma}{S}\right)^2, 1\right), \tag{29}$$

where h is calculated simply as the radius of the circle/sphere whose area equals that of the triangular/tetrahedral element Ω_i.

The Bx scheme and several of its variants have been used to compute hypersonic flow fields [49, 50, 48] with crisp shock capture and good convergence towards steady state properties. However, as we shall discuss in section 4, the dissipation that the Bx scheme provides across a strong, bow shock wave is *uneven* and may lead to perturbations in the post-shock region that eventually spoil the calculation [32, 43]. In upcoming sections we will consider strategies to devise better-behaved *RD* shock-capturing terms. In order to accomplish this goal, we need to delve first on the relation between *RD* schemes and stabilized finite element methods.

3.2. The Bx scheme as a stabilized shock-capturing FE method

Substituting relation (26) into equation (27) leads to:

$$\vec{\Phi}_l^{c,\Omega_i,Bx} = \vec{\Phi}_l^{c,\Omega_i,LDA} + \theta\vec{\delta}_l^{Diss,N}. \tag{30}$$

This expression makes evident how the first term $\vec{\Phi}_l^{c,\Omega_i,LDA}$ addresses the advection of smooth information, whereas the second term, locally active (*i.e.,* modulated by the shock detector), provides additional dissipation to handle strong gradients. In this sense, the Bx scheme in

DOI: 10.1002/fld

Eq. (30) can be seen as an *stabilized* finite element scheme supplemented with a shock-capturing term [10, 11, 12].

The relation existing between stabilized finite elements (*SUPG*) and residual distribution methods has been already pointed out in [51, 52, 19, 41, 53]. Indeed, the strong link between both approaches can be seen e.g. in the time-scales matrix τ_{SUPG} proposed in [54]: whenever τ_{SUPG} is particularized for a simplicial mesh and applied to an inviscid problem, a distribution matrix which is equivalent to the *RD* scheme termed *Lax-Wendroff* in [19] is obtained.

Once a link between *RD* and stabilized, shock-capturing schemes has been established, *importing* techniques from the *SUPG* framework into *RD* and vice versa becomes possible. In the next section we describe how to exploit this connection to retrieve shock-capturing terms with improved properties regarding total-enthalpy preservation at steady state.

3.3. Total enthalpy-preserving shock-capturing RD schemes

We begin by revisiting the *SUPG* shock-capturing term proposed by Kirk in [12].
In the spirit of the *FE* tradition (see e.g. [11]) Kirk introduces a supplementary artificial dissipative term into the Navier-Stokes equations:

$$\frac{\partial \vec{U}}{\partial t} + \nabla \cdot \bar{\bar{F}}^{c} = \nabla \cdot \bar{\bar{F}}^{d} + \nabla \cdot \bar{\bar{F}}^{ad}. \tag{31}$$

As usual, the artificial diffusion term is considered to be isotropic -*i.e.,* $\bar{\bar{F}}^{ad} = \mu^{art} \nabla \vec{W}$- and its contribution to the nodal updates is obtained through Galerkin discretization:

$$\vec{\delta}_l = \sum_{\Omega_i \in \Xi_l} \int_{\Omega_i} \mu^{art} \nabla N_l \cdot \nabla \vec{W} \, dv. \tag{32}$$

The novelty in Kirk's shock-capturing term lies in expressing $\bar{\bar{F}}^{ad}$ not in terms of the conserved variables $\vec{W}_1 = \vec{U}$ but in terms of a modified variable set $\vec{W}_2 \equiv [\rho, \, \rho\vec{u}, \rho H]^t$. This choice of variables is advantageous, as computations done with them mimic better important an physical property of the Euler equations (Eq. 16) at steady state, namely that total enthalpy is constant along streamlines [55], and consequently that the mass and total energy equations are proportional to each other [15].

In order to make explicit this last point, one needs first to identify which is the strong form that leads to Eq. 32 in each case. Using $\vec{W}_1$ implies that one is actually solving these conservation equations:

$$\nabla \cdot (\rho \vec{u}) = \nabla \cdot \left(\mu^{art} \nabla \rho \right), \tag{33a}$$

$$\nabla \cdot \left(\rho \vec{u} \cdot \vec{u}^t + p \bar{\bar{I}}_{n_D} \right) = \nabla \cdot \left(\mu^{art} \nabla \rho \vec{u} \right), \tag{33b}$$

$$\nabla \cdot (\rho H \vec{u}) = \nabla \cdot \left(\mu^{art} \nabla \rho E \right). \tag{33c}$$

DOI: 10.1002/fld

Using $\vec{W}_2$ substitutes the energy conservation equation (33c) in system above by:

$$\nabla \cdot (\rho H \vec{u}) \quad = \nabla \cdot (\mu^{art} \nabla \rho H) \,. \tag{34}$$

Expanding both equations (33c) and (34):

$$H \, \nabla \cdot (\rho \vec{u}) + \rho \vec{u} \cdot \nabla H = \begin{cases} E \, \nabla \cdot (\mu^{art} \nabla \rho) + \mu^{art} \rho \nabla \cdot (\nabla E) \,, \\ \\ H \, \nabla \cdot (\mu^{art} \nabla \rho) + \mu^{art} \rho \nabla \cdot (\nabla H) \,, \end{cases} \tag{35}$$

and using the fact that $\nabla H = \vec{0}$ for the case of a steady, adiabatic flow with uniform inflow, one observes how the energy conservation equation for $\vec{W}_2$ reduces to:

$$H \, \nabla \cdot (\rho \vec{u}) = H \, \nabla \cdot \left(\mu^{art} \nabla \rho \right) , \tag{36}$$

which is proportional to the mass conservation equation.

The discretized shock-capturing term corresponding to $\vec{W}_2 \equiv \vec{U}^H$ is given by [12]:

$$\vec{\delta}_l^H = \sum_{\Omega_i \in \Xi_l} \int_{\Omega_i} \mu^{art} \nabla N_l \frac{\partial \vec{U}^H}{\partial \vec{U}} \nabla \vec{U} \, dv. \tag{37}$$

In equation above, the scalar μ^{art} acts as a *shock-capturing function*, an operator based on the scaled norm of the *FE* residual at a given element; μ^{art} operates essentially as a shock detector function that modulates locally the contribution of the shock-capturing term.

In [12], Kirk showed how this shock-capturing term is capable of recovering practically the right pre-shock total enthalpy level for supersonic/hypersonic inviscid flow fields, in accordance with the physical behavior expected.

In this contribution, we introduce a new *RD* shock-capturing scheme by blending the classical LDA scheme and the stabilization term from the simple Lax-Friedrichs (or Rusanov) scheme [56, 57]. The corresponding element-to-node contribution of the $LDA + \delta^{LxF}$ scheme is given by:

$$\vec{\Phi}_l^{c,\Omega_i,LDA+LxF} = \vec{\Phi}_l^{c,\Omega_i,LDA} + \theta \vec{\delta}_l^{Diss,LxF}. \tag{38}$$

The explicit form of the stabilization term in *RD* form (see [20]) is:

$$\vec{\delta}_l^{Diss,LxF} = \max_{k \in \Omega_i} |\lambda_k| \sum_{m \in \Omega_i} \left(\vec{U}_l - \vec{U}_m \right) , \tag{39}$$

where λ_k are the eigenvalues in Equation (14).

In its current form, and as we shall see in section 4, the scheme does not recover the correct upstream total enthalpy levels. However, a variant of this scheme respecting better total enthalpy preservation

DOI: 10.1002/fld

can be built following the principles pointed out by Kirk. The element-to-node contribution of the total enthalpy preserving variant of the scheme, $LDA + \delta^{LxF,H}$, is:

$$\vec{\Phi}_l^{c,\Omega_i,LDA+LxF,H} = \vec{\Phi}_l^{c,\Omega_i,LDA} + \theta \frac{\partial \vec{U}^H}{\partial \vec{U}} \cdot \vec{\delta}_l^{Diss,LxF}. \tag{40}$$

In equation above, matrix $\frac{\partial \vec{U}^H}{\partial \vec{U}}$ is the Jacobian of the $\vec{U} - \vec{U}^H$ transformation:

$$\frac{\partial \vec{U}^H}{\partial \vec{U}} = \begin{bmatrix} 1 & 0 & 0 & 0 & 0 \\ 0 & 1 & 0 & 0 & 0 \\ 0 & 0 & 1 & 0 & 0 \\ 0 & 0 & 0 & 1 & 0 \\ \frac{1}{2}(\gamma-1)\|u\|^2 & -(\gamma-1)\,u & -(\gamma-1)\,v & -(\gamma-1)\,w & \gamma \end{bmatrix}, \tag{41}$$

where the velocity components u, v, w are those corresponding to the Roe averaged state.

One difference between the stabilized *FE* method of Kirk and our *RD* schemes lies in the definition of the shock detector: whereas μ^{art} in Equation (32) has residual character [12, 54], the shock detector θ in equation (28) has not. The modification to provide θ with residual character is straightforward; however, extensive experience with the detector of Dobeš shows that shock waves are captured crisply across few elements and fair convergence to steady state is obtained, see *i.e.,* [49, 50, 58, 48, 31, 32].

Finally, note that shock-capturing terms inspired on the median dual cell *RD* reformulation of *FV* flux functions(see [18]) could have also been employed. We have however preferred to favor the stabilized *FE* -*RD* over the *FV* -*RD* connection for two reasons: the first reason is the extreme sensitivity of most of *FV* flux functions to the inherent misalignment between numerical shock waves and the simplicial meshes we employ, as shown in [48]. This shortcoming might be alleviated by resorting to advanced *FV* flux functions that offer improved total-enthalpy preservation on unstructured grids (e.g. $AUSM + -up2$ and $LDFSS2001 - 2$ in reference [9]); however, the second reason to prefer the *RD* -stabilized *FE* parallelism has been the possibility of preserving the closest neighbor stencil for second-order accuracy, which is one of the main advantages of the *RD* framework.

4. INVISCID RESULTS

In this section we evaluate the performance of the schemes described in section 3.3 by computing hypersonic inviscid flows. Specifically, we investigate whether schemes $LDA + \delta^{LxF}$ and $LDA + \delta^{LxF,H}$ bring forward any advantage over the classical Bx scheme. We choose the inviscid blunt body problem as a benchmark to test the new schemes.

We consider first the hypersonic $Ma_\infty = 9$ inviscid flow around the mid-section of a infinitely long circular cylinder (1 unit length in diameter). Next, the robustness of the schemes considered

DOI: 10.1002/fld

is assessed on the same problem at $Ma_\infty = 18$. In both cases the uniform upstream conditions are $\rho_\infty = 1.4$, $p_\infty = 1$ and $u_\infty = -Ma_\infty$. A no penetration (slip wall) *BC* condition is enforced weakly at the cylinder surface; a supersonic inlet *BC* is imposed at the exterior curved boundary and supersonic outlet *BC* is considered at the remaining boundaries.

4.1. Inviscid $Ma_\infty = 9$ hypersonic flow around cylinder

The results presented in this section have been obtained with the Bx scheme in Eq. (30), with the $LDA + \delta^{LxF}$ scheme in Eq. (38) and with its total-enthalpy preserving variant $LDA + \delta^{LxF,H}$ scheme in Eq. (40). The solutions have been obtained in triangular meshes of resolution $n_T \times n_R = 121 \times 61$ nodes, *i.e.,* with $n_{Elem} \approx 1.44 \times 10^4$ and $n_{DoF} \approx 7.4 \times 10^3$ degrees of freedom, see Figure 3. All simulations are restarted from a 1^{st} order solution obtained with the N scheme. No sign of carbuncle was observed in these simulations [31].

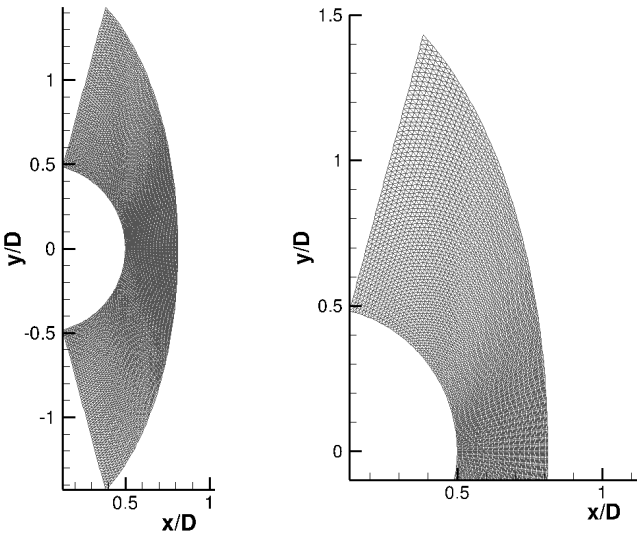

(a) Domain. (b) Detail.

Figure 3. Hypersonic inviscid $Ma_\infty = 9$ flow around cylinder: computational domain and mesh employed.

Figure 5 summarizes the Bx scheme results. The region where the N scheme dissipation -*i.e.,* the $\delta_l^{Diss,N}$ shock-capturing term- is active is shown in Fig. 5a: observe how the dissipation is applied in a very narrow region. Non-dimensional pressure field is shown in Fig. 5b: the strong compression across the bow shock is evident from the contour map scale. Despite the crisp shock-capture, the non-dimensional temperature field, shown in Fig. 5c, presents jagged iso-contours and shows the quite unexpected feature of having the hottest point in the immediate post-shock region but displaced vertically from the stagnation line. Note also the *contaminated* $1 - {}^{H}/_{H_\infty}$ field in Fig. 5d: errors in the post-shock total enthalpy in excess of 5% are visible. Finally, Fig. 5e shows that more

Prepared using fldauth.cls
DOI: 10.1002/fld

than 3000 iterations are necessary to have residuals decrease below 10^{-4} [§] .

Figure 6 gathers the results with the $LDA + \delta^{LxF}$ scheme. The δ_l^{LxF} stabilization term is active over the region shown in Fig. 6a: the dissipation is applied again in narrow region, though slightly larger than for the Bx scheme. Non-dimensional pressure field, see Fig. 6b, does not differ much from the Bx result and is somewhat smoother. The non-dimensional temperature field, shown in Fig. 6c, is free from the *jaggedness* afflicting the Bx solution; the post-shock region is unfortunately excessively smeared. The post-shock $1 - {}^{H}/_{H_\infty}$ field (Fig. 6d) is also smoother; however the correct upstream H_∞ is not recovered. Finally, observe how the solution residuals enter in a limit cycle. This behavior is characteristic of those situations where *excessive but uncontrolled* dissipation is introduced via a shock capturing term, see e.g. [31] for another example in the context of artificial viscous terms applied to prevent carbuncle instabilities.

Results obtained with the $LDA + \delta^{LxF,H}$ scheme are summarized in Figure 7. The $\delta_l^{LxF,H}$ stabilization term is active over an area of thickness comparable to the $LDA + \delta^{LxF}$ solution, see Fig. 7a The non-dimensional pressure field, see Fig. 7b, is also nearly indistinguishable from that of $LDA + \delta^{LxF}$. The non-dimensional temperature field, Fig. 7c, is on the contrary much better defined, and the hottest point is clearly located on the stagnation line. The post-shock $1 - {}^{H}/_{H_\infty}$ field (Fig. 7d) obtained with the $LDA + \delta^{LxF,H}$ scheme is smooth as well and the correct upstream H_∞ value is recovered away from the shock region. Finally, observe how the $LDA + \delta^{LxF,H}$ solution is obtained in around 700 iterations. This lends further support to the hypothesis advanced in [31], namely that the *quality* of the artificial dissipation applied -*i.e.,* the resemblance of the numerical dissipation to the physical diffusive operator- can be as important as its *intensity*.

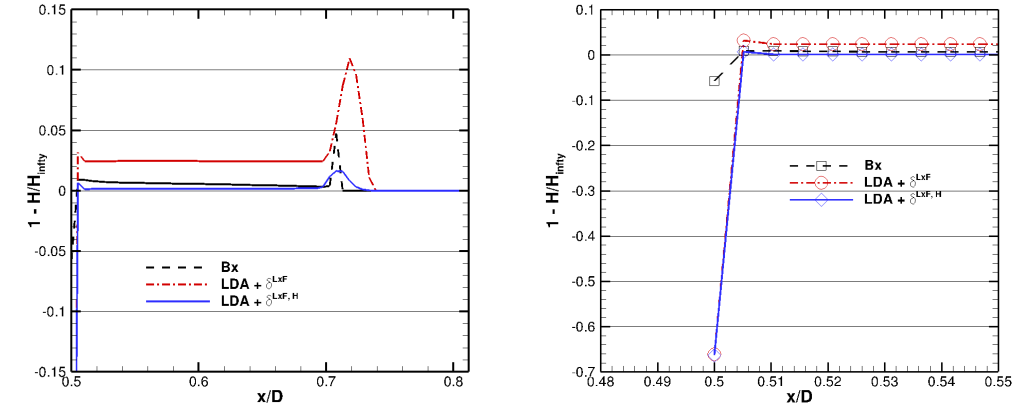

(a) Overall view.

(b) Detail, near stagnation point.

Figure 4. Hypersonic inviscid $Ma_\infty = 9$ flow around cylinder: $1 - {}^{H}/_{H_\infty}$ along stagnation line computed with Bx, $LDA + \delta^{LxF,H}$ and $LDA + \delta^{LxF,H}$ schemes.

[§]Solution does not change significantly if the solver is run till the residuals decrease below 10^{-4}.

DOI: 10.1002/fld

Figure 4 shows the evolution of $1 - {}^{H}/_{H_\infty}$ along the stagnation line for the three schemes considered in this work. The graph is consistent with the results described so far, namely, the Bx scheme provides insufficient dissipation to retrieve correct post-shock total enthalpy. On the contrary, the dissipation provided by the $LDA + \delta^{LxF}$ is excessive, and only the $LDA + \delta^{LxF,H}$ is able to retrieve the correct total-enthalpy level despite the same dissipation level is used.

Note finally how retrieving the correct total enthalpy at the stagnation point is problematic for all the three schemes considered (even for the $LDA + \delta^{LxF,H}$). Capturing the shock would not be then the only challenging feature for these kind of hypersonic flow fields; handling properly the stagnation point is also difficult [58, 48]. As conjectured in [43], this might be related with the fact that the eigenvector matrices R^U_m, L^U_m in Eq. 15 typically require, whenever $\vec{u} \cdot \vec{m} \to 0$, to be regularized by the addition of a small quantity $0 < \varepsilon \ll 1$ to the principal diagonal. This regularization could be compromising the solver performance at the stagnation point: in these situations the mesh topology in the neighborhood of the stagnation region is believed to be capable of impacting the solution quality.

DOI: 10.1002/fld

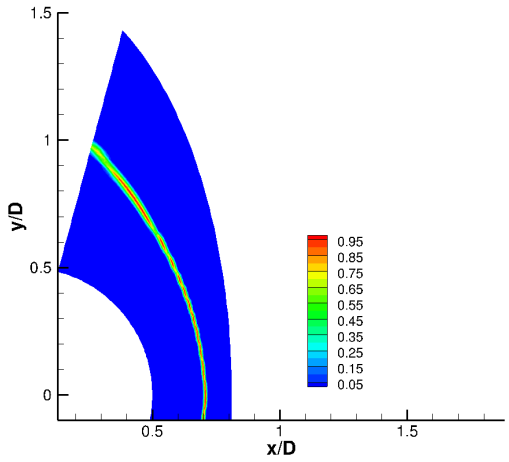

(a) Shock detector θ.

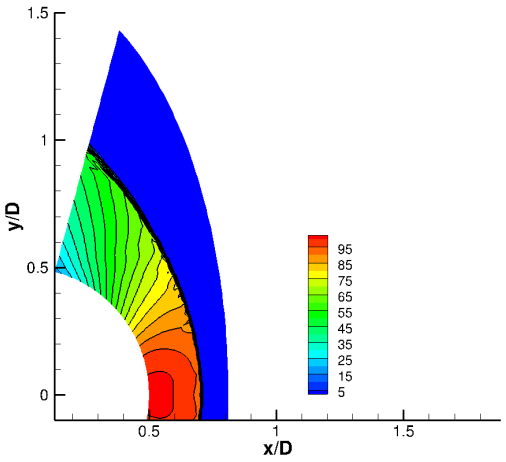

(b) p/p_∞ field.

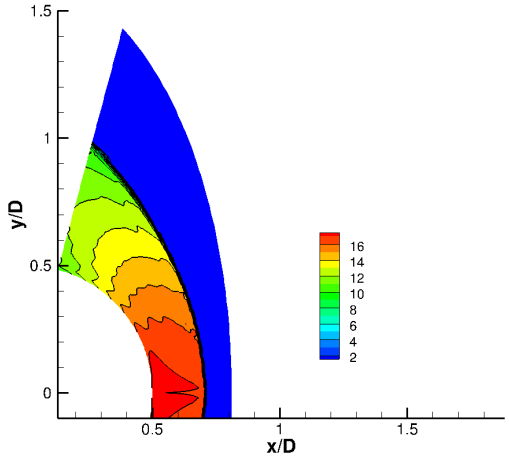

(c) T/T_∞ field.

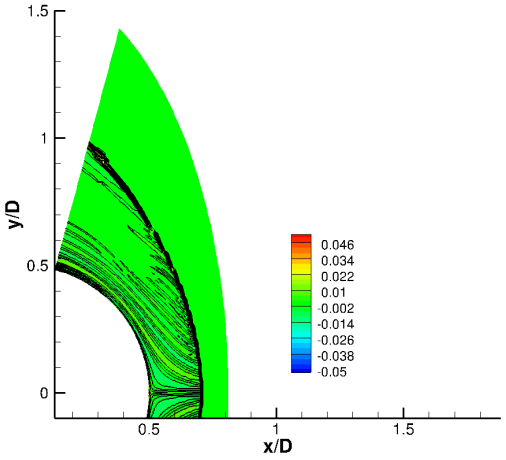

(d) $1 - H/H_\infty$ field.

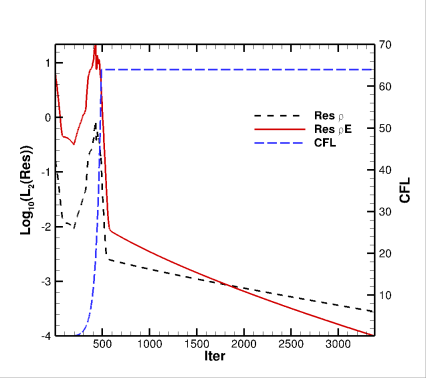

(e) Convergence history.

Figure 5. Hypersonic inviscid $Ma_\infty = 9$ flow around cylinder: Bx scheme solution ($S = 1$).

DOI: 10.1002/fld

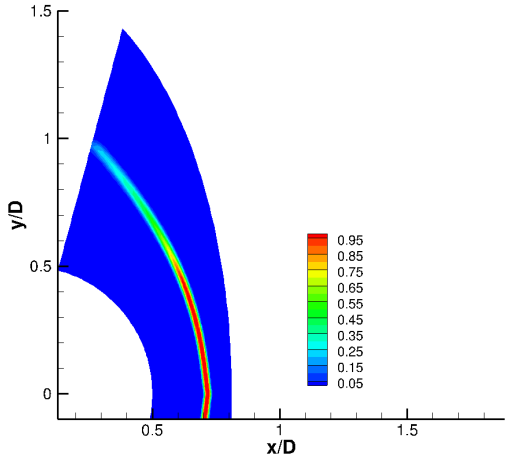

(a) Shock detector θ.

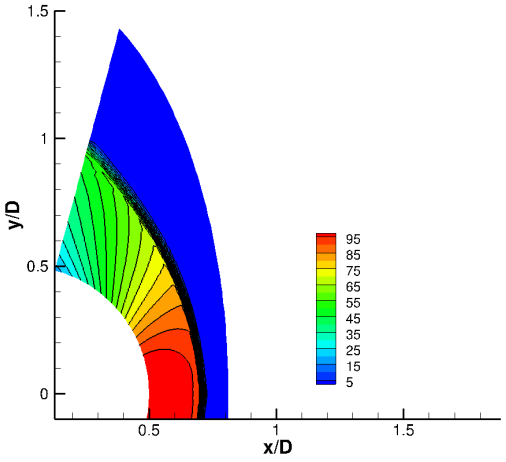

(b) p/p_∞ field.

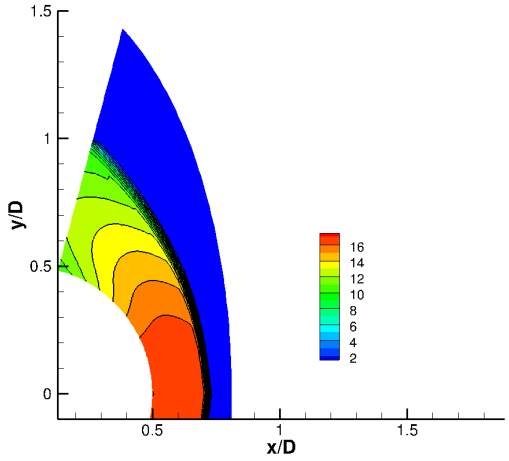

(c) T/T_∞ field.

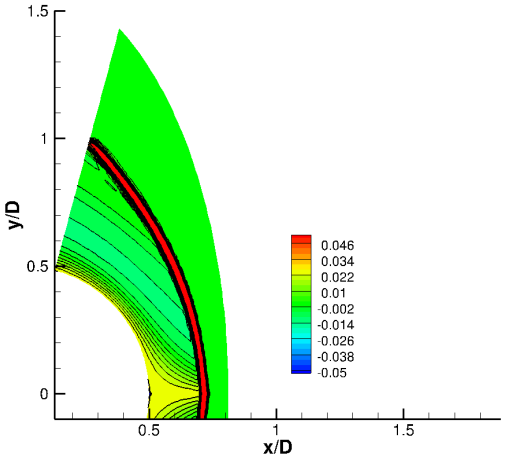

(d) $1 - H/H_\infty$ field.

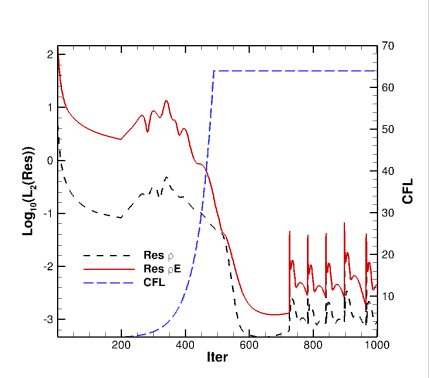

(e) Convergence history.

Figure 6. Hypersonic inviscid $Ma_\infty = 9$ flow around cylinder: $LDA + \delta^{LxF}$ scheme solution ($S = 8$).

Prepared using fldauth.cls
DOI: 10.1002/fld

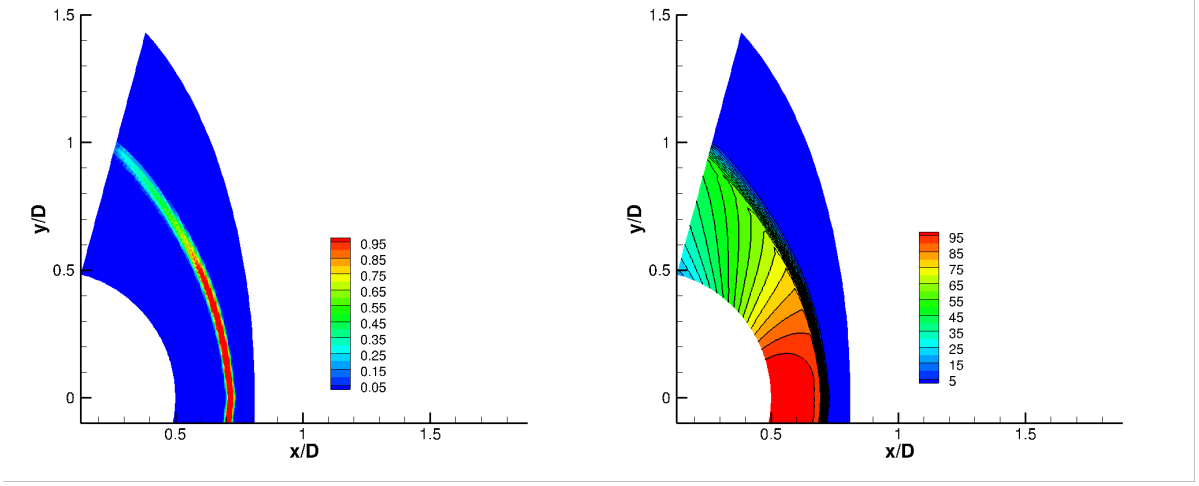

(a) Shock detector θ.

(b) p/p_∞ field.

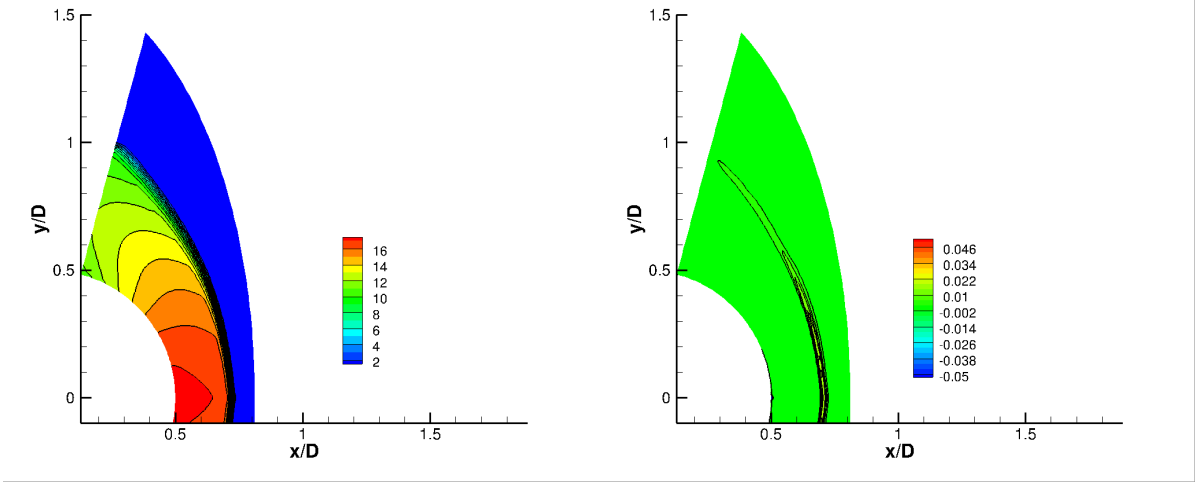

(c) T/T_∞ field.

(d) $1 - H/H_\infty$ field.

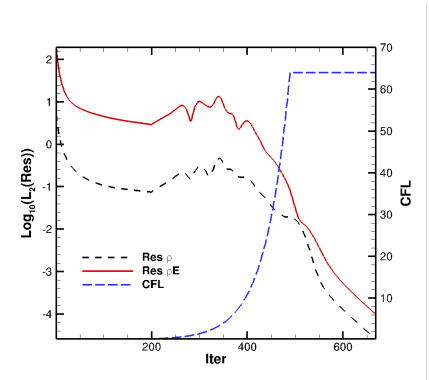

(e) Convergence history.

Figure 7. Hypersonic inviscid $Ma_\infty = 9$ flow around cylinder: $LDA + \delta^{LxF,H}$ scheme solution ($S = 8$).

DOI: 10.1002/fld

4.2. *Inviscid $Ma_\infty = 18$ hypersonic flow around cylinder*

In this section, we investigate whether the improved shock-capturing properties of the $LDA + \delta^{LxF,H}$ scheme carry on when facing stronger bow shock waves. The robustness of the scheme is thus assessed on an inviscid blunt body problem at $Ma_\infty = 18$.

Figure 8a shows the mesh employed in this case, consisting of $n_T \times n_R = 161 \times 61$ nodes, *i.e.,* with $n_{Elem} \approx 1.98 \times 10^4$ and $n_{DoF} \approx 1 \times 10^4$ degrees of freedom.

For this case, we have obtained solutions only with the Bx and the $LDA + \delta^{LxF,H}$ schemes; the $LDA + \delta^{LxF}$ scheme has not been considered, as we saw in the previous section that indiscriminate introduction of artificial dissipation is not effective in providing physically sound numerical solutions.

Regarding solutions obtained with the Bx scheme, similar observations as those in previous section apply. The corresponding plots have been therefore omitted to save space.

The $LDA + \delta^{LxF,H}$ solution is presented in Fig. 9. Here the remarks done in the previous section are also applicable: the pressure-field is wiggle free (Fig. 9b) and the hottest point is also located along the stagnation line (Fig. 9c). The upstream total enthalpy level is recovered in the post-shock region (Fig. 9d), and this time the behavior at the stagnation point is much better than in the previous case (see also Fig. 8b): this fact supports our conjecture of a possible influence of the mesh topology in the neighborhood of the stagnation point.

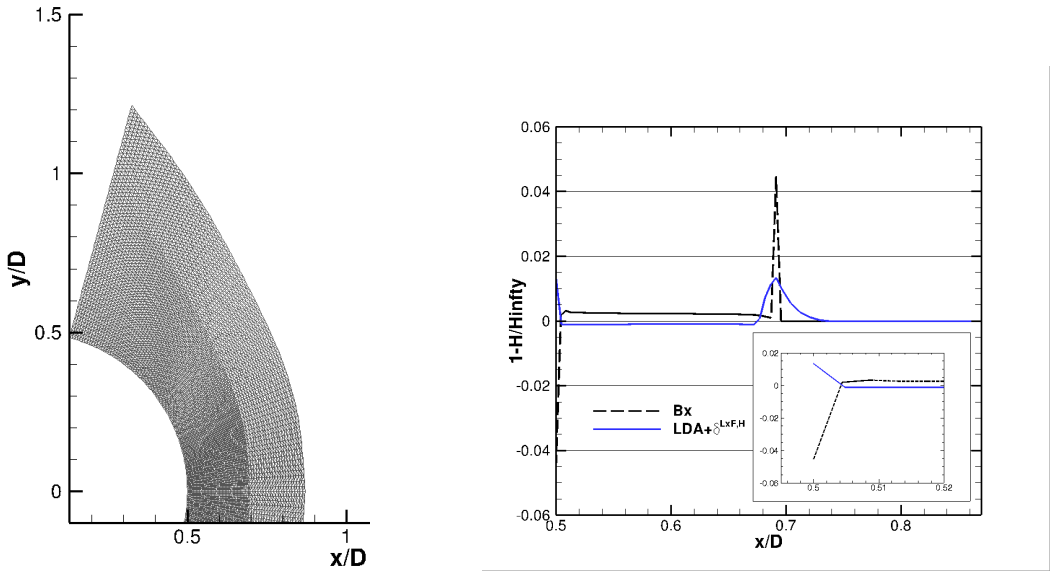

(a) (b)

Figure 8. Hypersonic inviscid $Ma_\infty = 18$ flow around cylinder: In (a), mesh employed; in (b) $1 - {}^{H}/_{H_\infty}$ along stagnation line computed with Bx and $LDA + \delta^{LxF,H}$ schemes.

DOI: 10.1002/fld

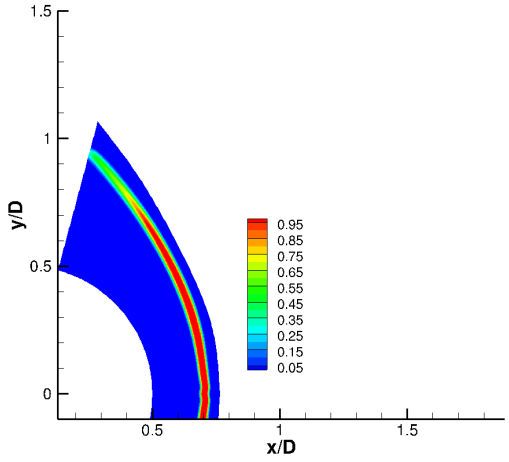

(a) Shock detector θ.

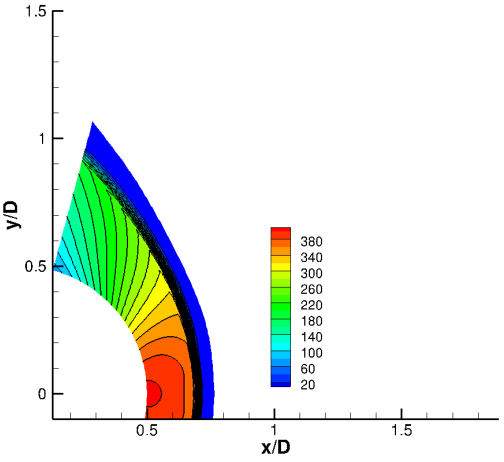

(b) p/p_∞ field.

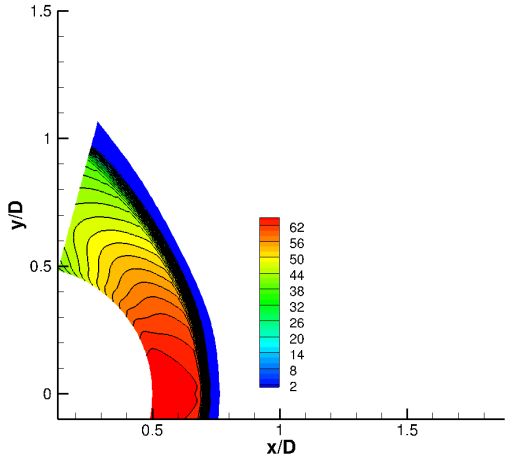

(c) T/T_∞ field.

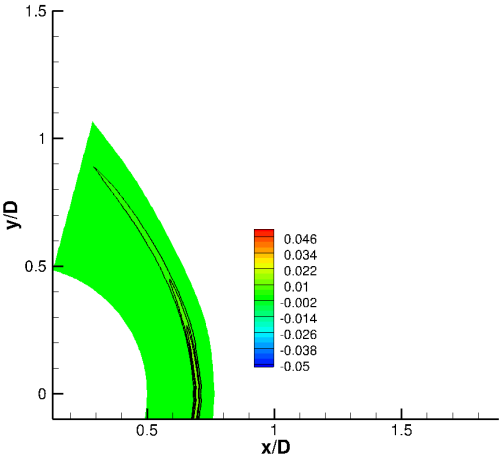

(d) $1 - H/H_\infty$ field.

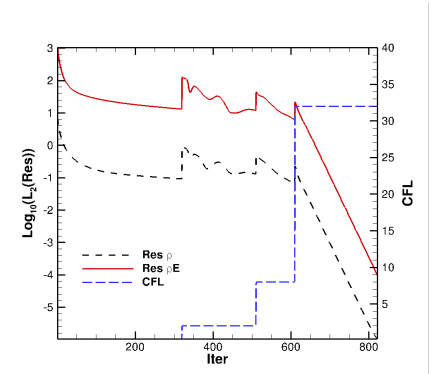

(e) Convergence history.

Figure 9. Hypersonic inviscid $Ma_\infty = 18$ flow around cylinder: $LDA + \delta^{LxF,H}$ scheme solution ($S = 11$).

DOI: 10.1002/fld

5. VISCOUS RESULTS

In this section we investigate how the $LDA + \delta^{LxF,H}$ scheme performs when applied to compute viscous hypersonic flow fields. We tackle first the hypersonic laminar boundary layer flow over an adiabatic flat plate in section 5.1, for which analytical solutions based on shock wave/boundary layer interaction theory are available. Next, in section 5.2, we consider the viscous counterpart of blunt body problem described in section 4.

5.1. *Hypersonic $Re_{L_d} = 10^5$ $Ma_\infty = 4.5$ flow over adiabatic flat plate*

We consider the $Re_{L_d} = 10^5$, $Ma_\infty = 4.5$ boundary layer (*BL*) flow over an adiabatic flat plate. Under these conditions the flow is laminar [59], the complexities of turbulence modeling are thus avoided. Hypersonic boundary layers typically modify the inviscid flow field beyond the *BL* edge, precisely because hypersonic boundary layers are relatively thicker (as $\delta_{BL}(x) \propto \frac{Ma^2}{\sqrt{Re_x}}$). Since the modified external inviscid flow affects in turn the *BL*, a viscous-inviscid interaction mechanism is established [37].

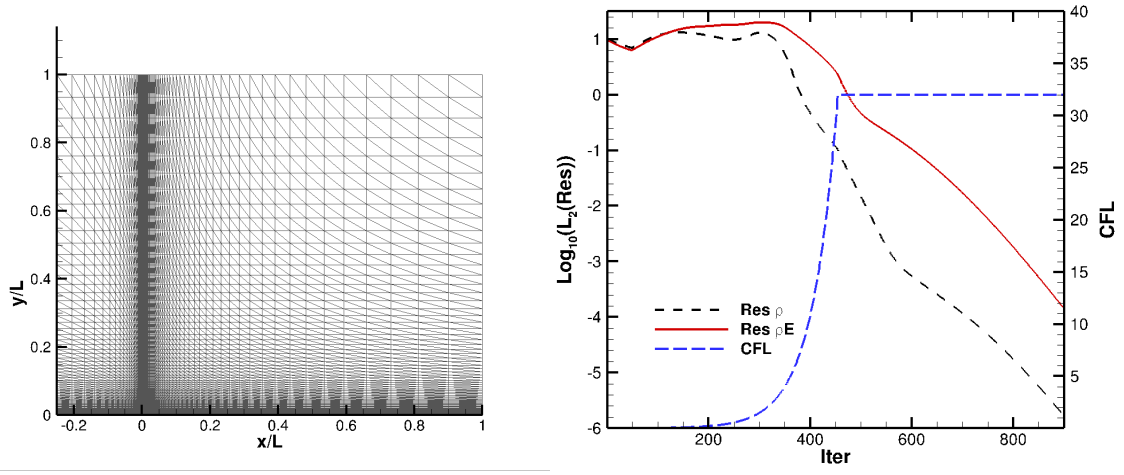

(a) Mesh.

(b) Convergence history for Bx.

Figure 10. Hypersonic $Ma_\infty = 4.5$, $Re_L = 1 \times 10^5$ flow over adiabatic flat plate: mesh and convergence history.

The computational domain is rectangular in shape, and extends $L_u = 0.4\,m$ upstream and $L_d = 1\,m$ downstream from the leading edge; the height of the domain is $H = 1\,m$. This domain has been discretized employing 120 (80 of them along the wall) nodes along the streamwise direction and 80 nodes in the transverse direction. The 1^{st} layer of interior nodes is $\delta = 0.5\,mm$ from the wall, see Fig. 10a.

The boundary conditions applied are:

- Surface $y = 0, x \in (0, L_d)$ is a no-slip adiabatic wall.
- Surface $x = L_d$ is a supersonic outlet.

DOI: 10.1002/fld

- Surfaces $x = -L_u$ and $y = H$ are supersonic inlets, with the upstream state set to the free stream value.
- Surface $y = 0, x \in (-L_u, 0)$ is considered a slip wall.

With these boundary conditions, the residuals decrease at least five orders of magnitude: see Figure 10b for the convergence history of the Bx scheme computations. The convergence history for the $LDA + \delta^{LxF,H}$ simulation is similar, and it is not shown here for reasons of space.

On preliminary computations considering a unit Prandtl number, the $LDA + \delta^{LxF,H}$ results improved marginally those obtained with the Bx scheme. For reasons of space, we have preferred to present only the results for the more physical $Pr = 0.71$ case, which are shown in Figure 11. The first remarkable feature is the different behavior of the schemes when faced with a straight attached shock wave in comparison to that of a detached bow shock wave. Both the Bx and the $LDA + \delta^{LxF,H}$ computations employ the same $S = 7$. Note how the shock detector is almost nowhere near 1. Indeed, and in order to discriminate better the regions where shock-capturing terms are active, Figures 11a and 11b show actually $\log(\max(\theta, 1 \times 10^{-12}))$: note how the dissipation is particularly important at the *root* of the shock wave.

Both the Bx and the $LDA + \delta^{LxF,H}$ schemes are capable of recovering the usptream total enthalpy level; notice also the progressive growth of the boundary layer thickness from the leading edge onwards.

We focus now on the wall pressure (Fig. 11e) and the skin friction (Fig. 11f) distributions obtained with both schemes. These distributions are compared against those predicted by the shock interaction theories described in [60]. These theories express quantities as boundary layer thickness, pressure, and skin friction in terms of the shock interaction parameter $\chi \propto \frac{Ma^3}{\sqrt{Re_x}}$. We will denote by $WI - 0th$, $WI - 1st$ and $WI - 2nd$ the distributions predicted by the Blasius solution with a Ma number correction [37], by the 1^{st} and by 2^{nd} order weak interaction theories presented in [60]. Note that the skin friction distribution given by the 2^{nd} order theory of Kubota and Ko [60] is known to overpredict largely C_f for flat plate configurations, as Carter pointed out in [61].

The Blasius solution with compressibility correction predicts a uniform non-dimensional pressure $p_W/p_{W,\infty}$ and a $x^{-0.5}$ variation for the C_f coefficient along the flat plate. Either of the interaction theories predicts, in the neighborhood of the leading edge, larger values of $p_W/p_{W,\infty}$ and C_f than those provided by corrected Blasius solution; as one moves further downstream all the three predictions coincide. Pressure for $WI - 1st$ and $WI - 2nd$ overlap from $\approx 100\,\mu m$ from the leading edge on.

Concerning the pressure distribution (Figs. 11e), the $LDA + \delta^{LxF,H}$ solution -after a shallow depression- begins to follow the trend of the $WI - 1st/WI - 2nd$ interaction theories just $\approx 2\,mm$ from the leading edge; the Bx solution lags slightly, and does not start following the interaction-theory-based predictions till $\approx 5\,mm$. As for the skin friction (Figs. 11f), both schemes begin to follow the $WI - 1st$ curve from $\approx 2mm$ on.

DOI: 10.1002/fld

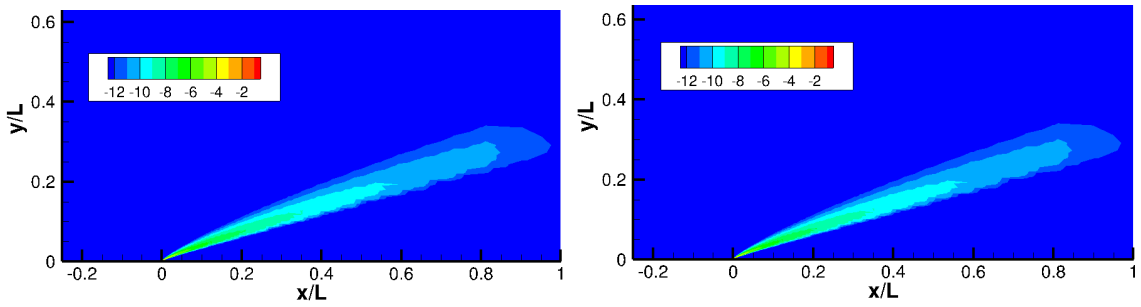

(a) Shock detector θ.

(b) Shock detector θ.

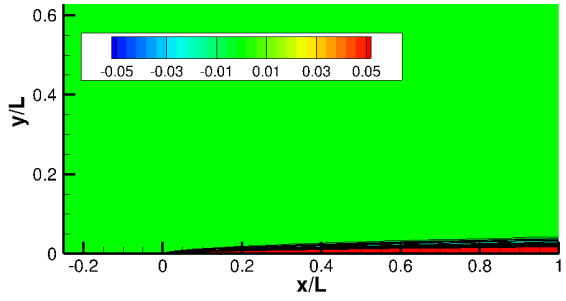

(c) $1 - {}^{H}/_{H_\infty}$ field.

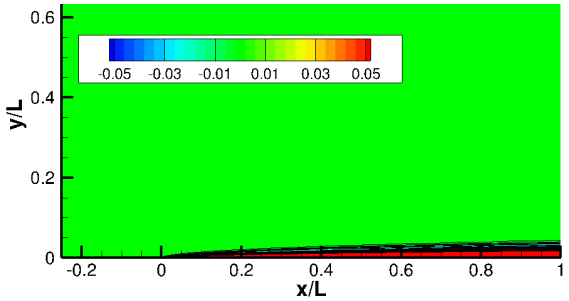

(d) $1 - {}^{H}/_{H_\infty}$ field.

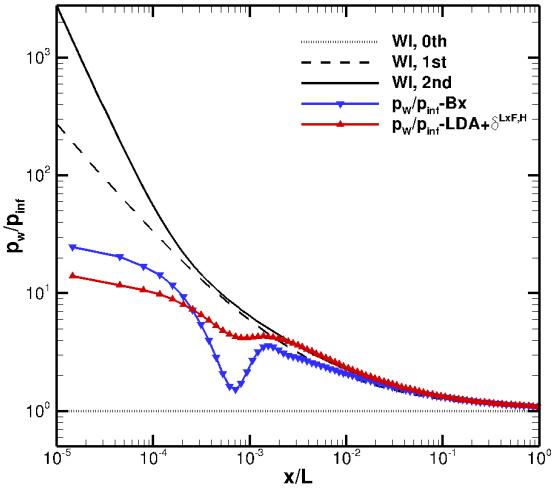

(e) Wall pressure.

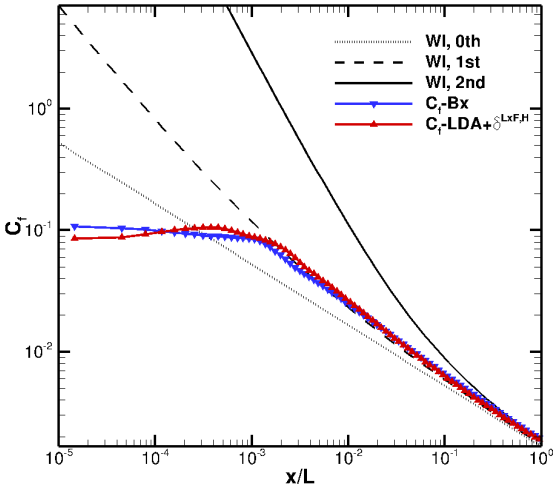

(f) Skin friction C_f

Figure 11. Hypersonic $Ma_\infty = 4.5, Re_L = 1 \times 10^5$ flow over adiabatic flat plate:
(a), (c) for Bx scheme ($S = 7$), while (b), (d) for $LDA + \delta^{LxF,H}$ scheme ($S = 7$). Wall quantities in (e) and (f).

DOI: 10.1002/fld

5.2. *Hypersonic* $Re_D = 2.6 \times 10^5$ $Ma_\infty = 8.1$ *flow around cylinder*

As a final testcase, the $Ma_\infty = 8.1$, $Re_D = 2.6 \times 10^5$ hypersonic viscous flow around a circular cylinder $40\,mm$ in diameter is considered. The upstream conditions are $T_\infty = 63.73K$, $p_\infty = 370.7Pa$ and $u_\infty = -1299.09\,m/s$; both adiabatic and isothermal ($T_w = 300\,K$) boundary conditions are considered at the wall. Fig. 12 shows the mesh employed, consisting of $n_T \times n_R = 161 \times 61$ nodes; stretching is applied from the wall onwards, with the first row of cells located at $1\,\mu\,m$ from the wall. Local refinement around the shock wave is also applied.

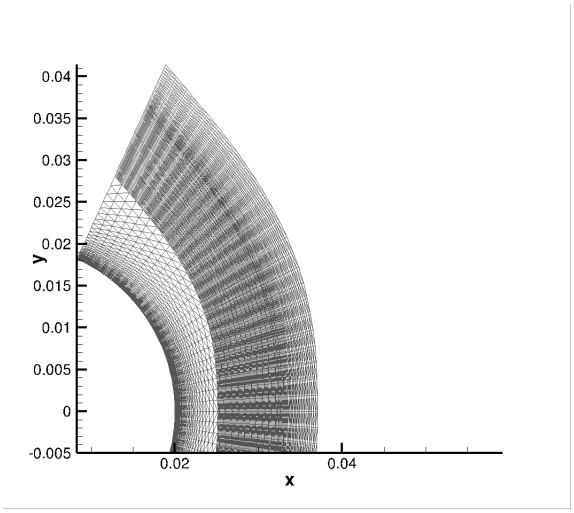

Figure 12. Hypersonic $Ma_\infty = 8.1, Re_D = 2.6 \times 10^5$ flow around adiabatic cylinder: mesh employed.

The adiabatic wall case has been simulated with both the Bx and the $LDA + \delta^{LxF,H}$ schemes. Figures 14 and 15 gather the results computed with both schemes. Contrarily to what we observed for the hypersonic flat plate case, the schemes behave radically different when faced with a bow shock. This difference in behavior is consistent with the remarks made in section 4.

The shock is captured around a very narrow region (Fig. 14a) when the Bx scheme is employed. Overall, the pressure field is well described, Fig. 14b; but one cannot say the same neither for the temperature (Fig. 14c) nor for the enthalpy fields, Fig. 14d. This computation has needed around 2100 iterations to reach convergence, Fig. 14f.

Figure 14e presents the wall pressure distribution (adimensionalized with the Pitot pressure $p_{10} = 31472.43\,Pa$) by the Bx scheme and compares it against the *FV* prediction for the isothermal case provided in reference [9]. The adequacy of this comparison will be justified when describing Figure 13a; for now let us comment that despite all the flaws visible in the flow field, the Bx scheme is capable of providing an acceptable pressure distribution almost everywhere but in the neighborhood of the stagnation point: there we observe a slight discrepancy with the *FV* solution. We defer the comments on the skin friction till we have presented the $LDA + \delta^{LxF,H}$ solution.

DOI: 10.1002/fld

Figure 15 gathers the information relative to the $LDA + \delta^{LxF,H}$ solution. As usual, the shock-capturing term is active in a region slightly thicker than for the Bx scheme (Fig. 15a). The pressure and temperature fields are nevertheless well represented and not *overdiffused*, see Fig. 15b and 15c. Moreover, the hottest point is once again along the stagnation line. The wall pressure distribution follows closely the FV reference solution, and only about 1100 iterations were needed to obtain this solution.

We proceed now to justify the appropriateness of using the isothermal FV prediction of the wall pressure as reference for our adiabatic calculations. Figure 13a shows the p_w/p_{01} distribution as computed with $LDA + \delta^{LxF,H}$ using both an adiabatic and an isothermal ($T_w = 300\,K$) wall boundary conditions: both curves overlap.

Concerning skin friction prediction, Figure 13b shows the C_f distribution predicted by the Bx and the $LDA + \delta^{LxF,H}$ schemes. Both solutions are relatively close to each other over most of the wall; however, the Bx scheme prediction is not antisymmetric at the stagnation point, as one would expect. The $LDA + \delta^{LxF,H}$ scheme makes, on the contrary, a better job at respecting the antisymmetry condition at $y = 0$. This behavior is then another demonstration that it is worth investing into shock-capturing terms that are as consistent with the physics as possible.

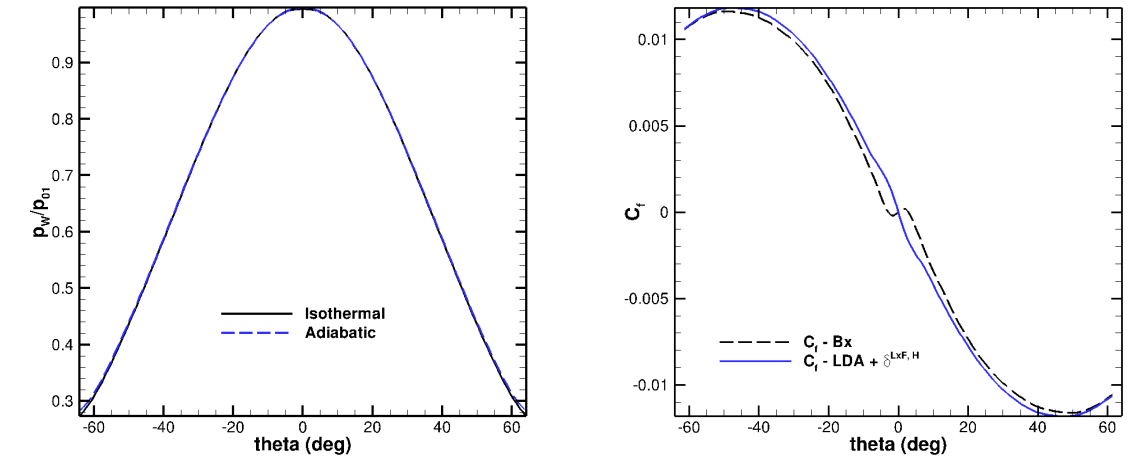

(a) (b)

Figure 13. Hypersonic $Ma_\infty = 8.1, Re_D = 2.6 \times 10^5$ flow around cylinder:
(a) Wall pressure for the adiabatic and the isothermal cases computed with $LDA + \delta^{LxF,H}$ scheme.
(b) Skin friction C_f for Bx and $LDA + \delta^{LxF,H}$ schemes.

We gather the results obtained with the $LDA + \delta^{LxF,H}$ scheme for the isothermal ($T_w = 300\,k$) case in Figure 16. Pressure (Fig. 16a) and temperature (Fig. 16b) fields are not much different from those retrieved in the adiabatic wall case. The $LDA + \delta^{LxF,H}$ scheme does also a good work in recovering the correct upstream total enthalpy level in the post-shock region, Fig. 16c.

DOI: 10.1002/fld

Finally, Figure 16f compares the $LDA + \delta^{LxF,H}$ heat flux prediction against the *FV* prediction in [9]. Heat flux has been non-dimensionalized with the value given by the Fay-Ridell relation $q_{FR} = 17.5\, W/cm^2$, see [37]. The $LDA + \delta^{LxF,H}$ heat flux prediction is, unfortunately, far from the reference solution: two symmetric *humps* appear away from the stagnation point. The Bx prediction is also shown for comparison: in this case an underprediction of the heating at the stagnation point is visible. Again, we believe that the regularization of the left/right eigenvector matrices in Eq. 15 might be at the root of this behavior.

Finally, note that *FV* computations with the Roe flux function with entropy-correction and `MUSCL` reconstruction, described in [8], report similar anomalies in heating prediction.

DOI: 10.1002/fld

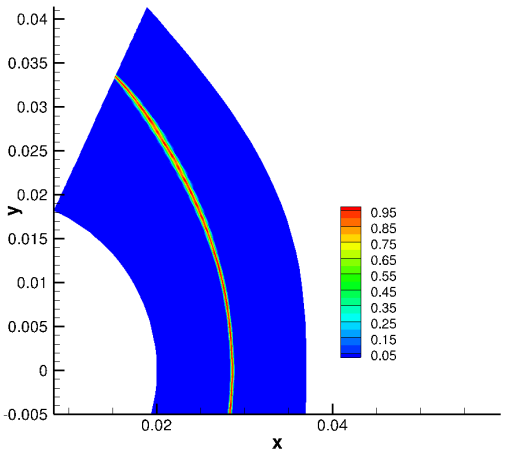

(a) Shock detector θ.

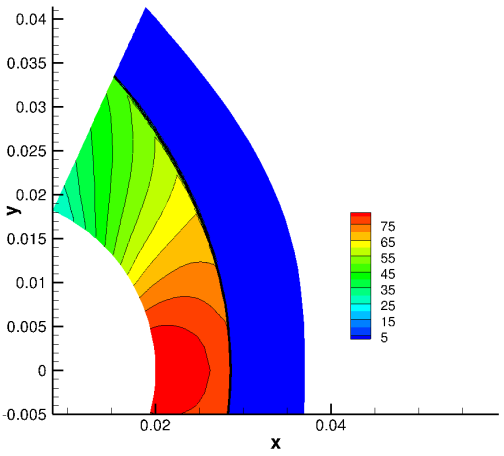

(b) p/p_∞ field.

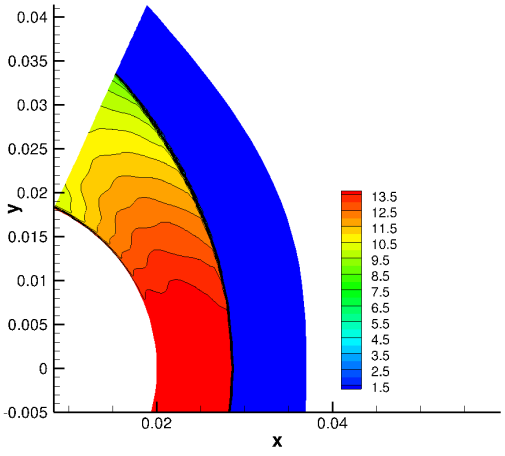

(c) T/T_∞ field.

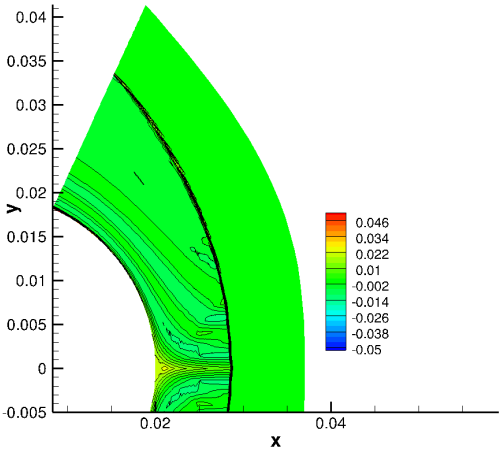

(d) $1 - H/H_\infty$ field.

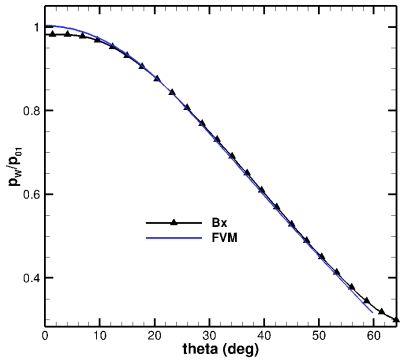

(e) Wall pressure (*FV* prediction from [9]).

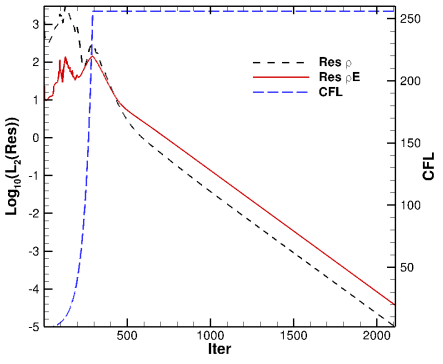

(f) Convergence history.

Figure 14. Hypersonic $Ma_\infty = 8.1, Re_D = 2.6 \times 10^5$ flow around adiabatic cylinder: Bx scheme solution ($S = 30$).

Prepared using fldauth.cls
DOI: 10.1002/fld

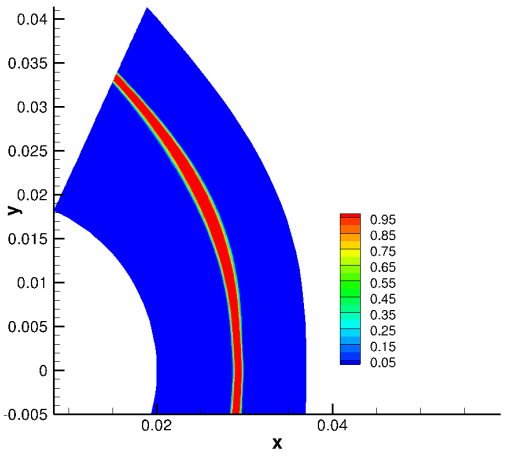

(a) Shock detector θ.

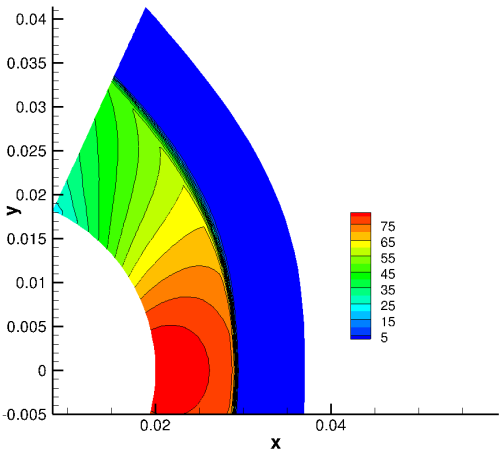

(b) p/p_∞ field.

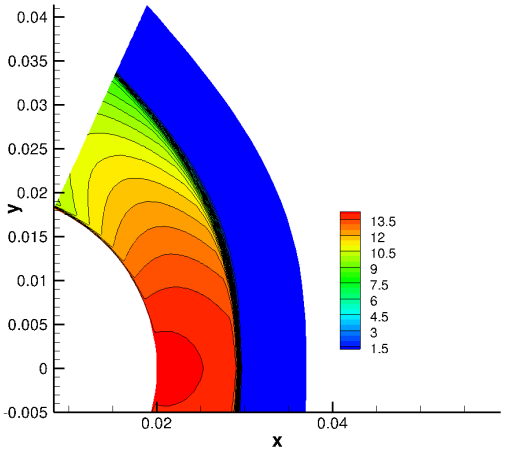

(c) T/T_∞ field.

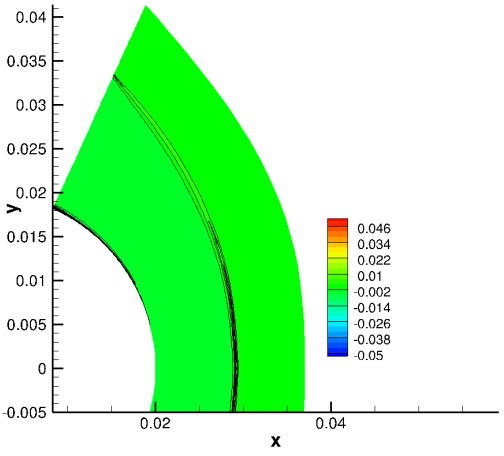

(d) $1 - H/H_\infty$ field.

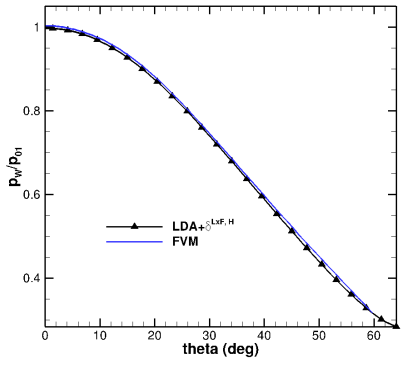

(e) Wall pressure (*FV* prediction from [9]).

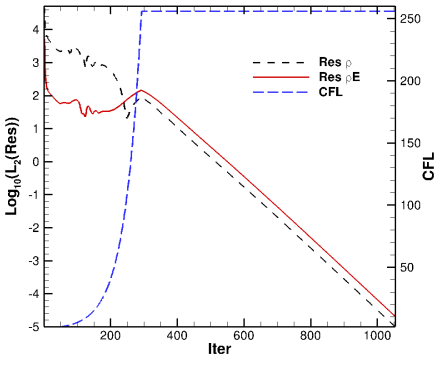

(f) Convergence history.

Figure 15. Hypersonic $Ma_\infty = 8.1, Re_D = 2.6 \times 10^5$ flow around adiabatic cylinder: $LDA + \delta^{LxF,H}$ scheme solution ($S = 30$).

DOI: 10.1002/fld

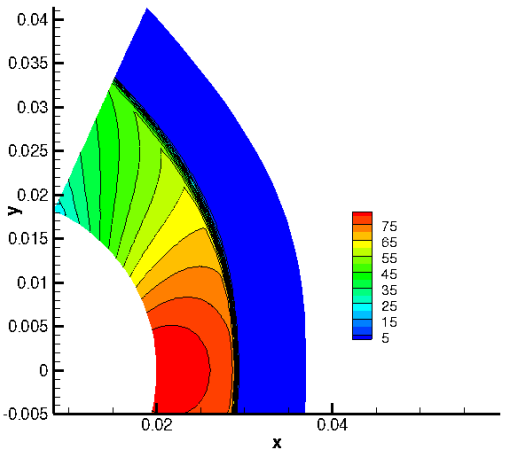

(a) p/p_∞ field.

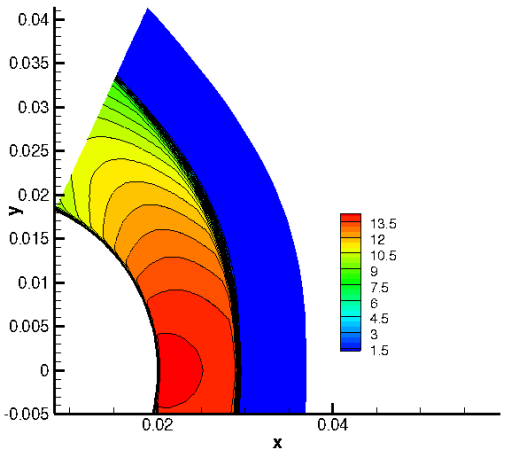

(b) T/T_∞ field.

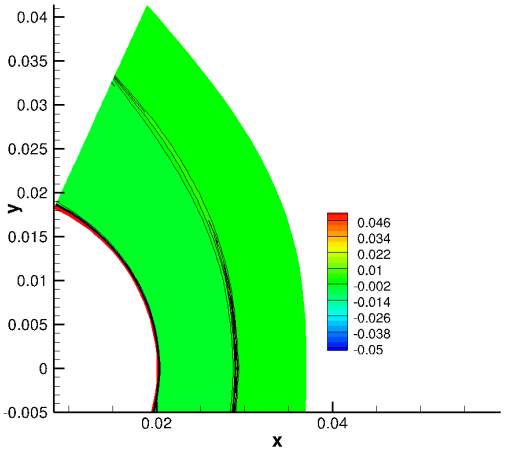

(c) $1 - H/H_\infty$ field.

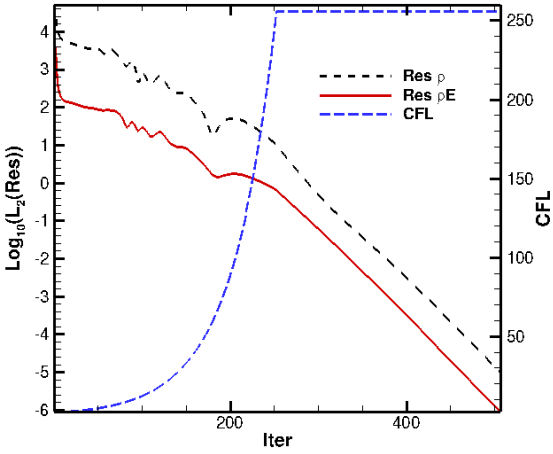

(d) Convergence history.

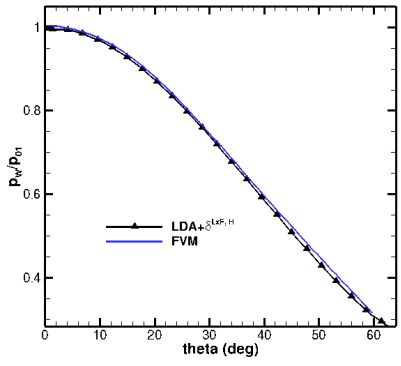

(e) Wall pressure.

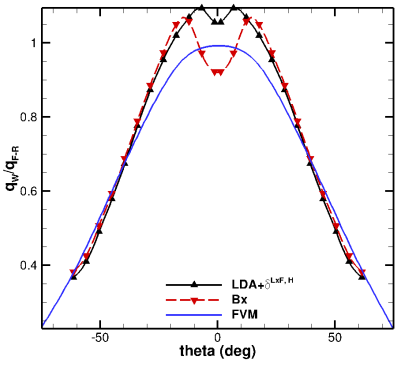

(f) Heat transfer.

Figure 16. Hypersonic $Ma_\infty = 8.1$, $Re_D = 2.6 \times 10^5$ flow around isothermal cylinder: $LDA + \delta^{LxF,H}$ scheme solution ($S = 30$).

Prepared using fldauth.cls
DOI: 10.1002/fld

6. CONCLUSIONS

In this contribution we have devised an enthalpy preserving shock-capturing term. This novel term allows, in combination with a multidimensional upwind residual distribution scheme, to compute hypersonic steady flow fields with strong bow shock waves in a robust manner while recovering the correct upstream total enthalpy level.

This shock-capturing term has been derived by exploiting a known -but so far relatively unexplored- parallelism between stabilized finite element techniques and residual distribution methods.

The shock-capturing term has been built around the Lax-Friedrichs stabilization term, which is *possibly* the most simple dissipative term available in the residual distribution method framework. The new scheme can be implemented into existing codes with minimally invasive changes, and is compatible with other shock-stabilizing terms, e.g. those described in [62, 31].

The performance of the improved shock-capturing term combined with the LDA scheme (termed $LDA + \delta^{LxF,H}$ scheme) has been evaluated on both inviscid and viscous hypersonic flow problems presenting both attached and detached shock waves. In all cases considered the shock-capturing term is capable of recovering the correct upstream total enthalpy level. Solutions obtained with the $LDA + \delta^{LxF,H}$ scheme present less wiggles, better post-shock temperature fields and converge faster towards the steady state than those obtained with the classical Bx scheme of [42].

The favorable properties of the new shock-capturing term are preserved as well when applied to viscous simulations: both wall pressure and skin-friction predictions obtained with the $LDA + \delta^{LxF,H}$ scheme improve those obtained with the classical Bx scheme.

The enthalpy preserving shock-capturing term has, unfortunately, a limited effect on heat transfer predictions. Solutions with the $LDA + \delta^{LxF,H}$ scheme improve only marginally those obtained with the Bx scheme. A conjecture regarding a possible degeneracy of the LDA scheme that is employed in the smooth parts of the flow field has been proposed .

In this contribution we have exploited the shock-capturing term in combination with the multidimensional upwind LDA residual distribution scheme. However, nothing in the formulation employed prevents to combine the shock-capturing term in combination with other residual distribution schemes, or with Finite Volume [63], Stabilized Finite Element [12] or Discontinuous Galerkin [14, 13] schemes.

ACKNOWLEDGEMENTS

First author has been supported by the NNATAC FP7 initiative (PIAP-GA-2012-324298) and by the European Commission Research and Innovation action DRAGY (Grant Agreement 690623).

The authors thankfully acknowledge the computer resources, technical expertise and assistance provided by the Supercomputing and Visualization Center of Madrid (CeSViMa).

DOI: 10.1002/fld

A. FURTHER DETAILS ON RESIDUAL DISTRIBUTION SCHEMES

Additional details on the residual distribution solver employed in this work are provided in this appendix.

A.1. Diffusive residual

Note that the components of the diffusive flux tensor, $\vec{F}_j^v$ depend not only on the solution $\vec{U}$ but on its gradient as well:

$$\vec{F}_j^v = f\left(\mu, \lambda, \vec{U}, \nabla\vec{U}\right). \tag{42}$$

The discretization of the diffusive flux tensor $\vec{F}_j^v$ using $P1$ finite elements is accomplished as [42]:

$$\vec{\Phi}_l^d = \int_\Omega N_l \frac{\partial \vec{F}_j^v}{\partial x_j}\, dv = \int_{\Xi_l} N_l \frac{\partial \vec{F}_j^v}{\partial x_j}\, dv = \sum_{\Omega_i \in \Xi_l} \int_{\Omega_i} N_l \frac{\partial \vec{F}_j^v}{\partial x_j}\, dv. \tag{43}$$

Integrating expression above by parts and applying the Gauss-Ostrogradsky theorem leads to:

$$\vec{\Phi}_l^d = \oint_{\Xi_l \cap \delta\Omega} N_l \vec{F}_j^v 1_j^{ext} ds - \sum_{\Omega_i \in \Xi_l} \int_{\Omega_i} \frac{\partial N_l}{\partial x_j} \vec{F}_j^v\, dv. \tag{44}$$

First term on the *RHS* of last equation is different from zero only for those elements lying on the external boundary, $\delta\Omega \cap \Xi_l \neq \emptyset$. The diffusive contributions to residual of interior nodes are collected into the second term of the *RHS* . The corresponding discrete form for a $P1$ linear element is:

$$\vec{\Phi}_l^d = -\sum_{\Omega_i \in \Xi_l} \frac{1}{2} n_{j,l} \vec{F}_j^v \left(\mu_{avg}, \lambda_{avg}, \vec{U}_{avg}, \nabla\vec{U}^h\right). \tag{45}$$

Treatment of the diffusive flux tensor $\vec{F}_j^v$ as in equation (45) rests into the variational formulation presented in [64]. This formulation employs test functions given by:

$$\omega_l = N_l + \sum_{\Omega_i \in \Xi_l} \left(3\, B_l^{\Omega_i} - \bar{\bar{I}}_{nEqs}\right) \mathfrak{B}^{\Omega_i}. \tag{46}$$

In expression above $\mathfrak{B}^{\Omega_i}$ is a piecewise linear bubble-function that takes unit value at the centroid of Ω_i and 0 at the contour $\delta\,\Omega_i$.

This choice of the test functions allows to reconcile the Galerkin discretization of the diffusive term described in equation (45) and the *RD* discretization of the advective part presented in section 3.

A.2. Boundary conditions

References [65, 27] detail how boundary conditions are enforced in the context of residual distribution schemes. Here, we cover briefly the difference between *strong* and *weak* imposed boundary conditions and its relation to the limited subset of *BC*'s employed in this work.

A boundary condition is imposed *strongly* when the *a priori* known value of the solution is substituted into Eq. 18, so that:

$$\vec{U}^h(\vec{x}, t) = \sum_{j \in \delta\Omega^{h,D}} \vec{U}_j^{BC} N_j(\vec{x}) + \sum_{j \in \Omega^h - \delta\Omega^{h,D}} \vec{U}_j N_j(\vec{x}). \tag{47}$$

Alternatively, *BC*'s can be enforced *weakly*, introducing a *corrective* residual $\vec{\Phi}_l^{BC}$ to equation (20). This $\vec{\Phi}_l^{BC}$ is conceived so that the solution $\vec{U}_l$ at steady state reduces to the requested value $\vec{U}_l^{BC}$. The rationale

Prepared using fldauth.cls
DOI: 10.1002/fld

for this technique departs from the weak formulation of the problem:

$$\int_{\Omega} \omega_l \frac{\partial \vec{F}_j}{\partial x_j}\, dv = \vec{0}.$$

Integration by parts, use of Gauss-Ostrogradsky theorem, and a second integration by parts step yield:

$$\int_{\Omega} \omega_l \frac{\partial \vec{F}_j}{\partial x_j}\left(\vec{U}^h\right) dv + \underbrace{\oint_{\delta\Omega} \omega_l \left[\vec{F}_j\left(\vec{U}^{h,BC}\right) - \vec{F}_j\left(\vec{U}^h\right)\right] 1_j^{ext} ds}_{\vec{\Phi}_l^{BC}} = \vec{0}. \tag{48}$$

Discretization of interior points is recovered but now with boundary contributions made explicit. Equation (48), cast in linearized form, reads:

$$\vec{\Phi}_l^{BC} = \sum_{S_f \in \delta\Xi_l \cap \delta\Omega} \int_{S_f} \omega_l^{\delta\Omega_i} A_j^{c,U}\left(\vec{U}^{h,BC} - \vec{U}^h\right) 1_j^{ext} ds = K_l \cdot \left(\vec{U}_l^{BC} - \vec{U}_l^h\right). \tag{49}$$

Since *RD* schemes are vertex-centered numerical techniques, strong imposition of boundary conditions is straightforward at those boundary nodes where the solution is fully known a priori, *i.e.,* at supersonic inlets and no-slip (adiabatic/isothermal) walls. Nodes at a supersonic outlet region are treated as interior points, which is consisteng with having the characteristic lines exiting the domain.

Conversely, whenever the state vector cannot be defined unambiguously neither from the interior solution nor from external information, weak enforcement of the boundary condition is the natural alternative, specially if the *upwind projector* K_l^+ is used in Eq. (49) instead of K_l. The *upwind projector* discriminates information entering the domain while discards contributions associated to outgoing characteristics. Inviscid walls are enforced weakly through Eq. (48). The flow tangency condition is imposed by specifying:

$$\Delta\vec{F}_j^c \equiv \vec{F}_j^{c,BC} - \vec{F}_j^{c,h} = -\left[\rho\, u_n, \rho\, u_j\, u_n, \rho E\, u_n\right]^t. \tag{50}$$

Symmetry is achieved simply by setting the vertical velocity component v to 0 in $\vec{U}_l^{BC}$, see [19].

A.3. Numerical solution of the discretized set of equations

Since system of equations (1) is of mixed parabolic-hyperbolic type, [1], its steady solution can be obtained marching in pseudo-time. The distribution procedure described in sections 3 and A.1 results into a system of ordinary differential equations describing the time evolution of the solution at the grid nodes. For the l-th node, this system reads:

$$V_{\Xi_l} \frac{d\vec{U}_l}{dt} + \vec{\Phi}_l^c - \vec{\Phi}_l^d = \vec{0}, \tag{51}$$

where V_{Ξ_l} stands for the volume of the median dual cell around l-th node.

The discretization of Eq. (51) is accomplished by means of the `COOLFluiD` solver, described in [66]. Equation (51) is advanced in pseudo-time by using an implicit backward Euler integrator, until a steady state solution is reached. At each *pseudo-time* step a linear system of equations needs to be solved: this is accomplished by the `GMRES` Krylov subspace method [67] provided by the `PETSc` solver library [68].

DOI: 10.1002/fld

References

1. Hirsch C. *Numerical Computation of Internal and External Flows: Introduction to the Fundamentals of CFD, 2^{nd} Edition*. Butterworth-Heinemann, 2006.
2. Leveque R. *Finite Volume Methods for Hyperbolic Problems*. Cambridge University Press, 2002.
3. Von Neumann J, Richtmyer RD. A Method for the Numerical Calculation of Hydrodynamic Shocks. *Journal of Applied Physics* Mar 1950; **21**:232–237, doi:10.1063/1.1699639.
4. Salas M. *A Shock-Fitting Primer, $3^{rd}Ed$.* CRC Press, 2009.
5. Roe P. Approximate Riemann Solvers, Parameter Vectors, and Difference Schemes. *J. Comput. Physics* 1981; **43**:357–372.
6. Yee H, Klopfer G, Montagné JL. High-resolution shock-capturing schemes for inviscid and viscous hypersonic flows. *Journal of Computational Physics* 1990; **88**(1):31 – 61, doi:https://doi.org/10.1016/0021-9991(90)90241-R. URL http://www.sciencedirect.com/science/article/pii/002199919090241R.
7. Jameson A, Schmidt W, Turkel E. Numerical solution of the Euler equations by finite volume methods using Runge–Kutta time stepping schemes. No. AIAA 1981–1259, AIAA 14^{th} Fluid and Plasma Dynamics Conference in Fluid Dynamics and Colocated Conferences, American Institute of Aeronautics and Astronautics, 1981, doi: 10.2514/6.1981-1259. URL https://doi.org/10.2514/6.1981-1259.
8. Kitamura K, Shima E, Nakamura Y, Roe P. Evaluation of Euler fluxes for hypersonic flow computations. *AIAA Journal* 2010; **48**(4):763–776.
9. Kitamura K, Shima E. Towards shock-stable and accurate hypersonic heating computations: A new pressure flux for AUSM-family schemes. *J. Comput. Physics* 2013; **245**:62–83.
10. Hughes T, Mallet M. A new finite element formulation for computational fluid dynamics: III. the generalized streamline operator for multidimensional advective-diffusive systems. *Computer Methods in Applied Mechanics and Engineering* 1986; **58**(3):305–328.
11. Hughes T, Mallet M. A new finite element formulation for computational fluid dynamics: IV. a discontinuity-capturing operator for multidimensional advective-diffusive systems. *Computer Methods in Applied Mechanics and Engineering* 1986; **58**(3):329–336.
12. Kirk BS. Adiabatic shock capturing in perfect gas hypersonic flows. *International Journal for Numerical Methods in Fluids* 2010; **64**:1041–1062.
13. Persson P, Peraire J. Sub-cell shock capturing for discontinuous Galerkin methods. *AIAA paper* 2006; **112**:2006.
14. Barter E, Darmofal D. Shock capturing with PDE-based articial viscosity for DGFEM: Part I. Formulation. *J. Comput. Physics* 2010; **229**:1810–1827, doi:10.1016/j.jcp.2009.11.010.
15. Jameson A. Analysis and design of numerical schemes for gas dynamics. 2: artificial diffusion and discrete shock structure. *Technical Report CR–196476*, NASA 1994.
16. Ciccoli M, Desideri JA. Numerical computations of steady homenthalpic non-equilibrium flows. *Computers & Fluids* 1995; **24**(6):719 – 737, doi:https://doi.org/10.1016/0045-7930(95)00011-Z. URL http://www.sciencedirect.com/science/article/pii/004579309500011Z.
17. Persson P. Shock capturing for high-order discontinuous Galerkin simulation of transient flow problems. *21st AIAA Computational Fluid Dynamics Conference*, 2013; 3061.
18. Abgrall R. Toward the ultimate conservative scheme: Following the quest. *International Journal for Numerical Methods in Fluids* 2001; **167**:277315.
19. van der Weide E. Compressible flow simulation on unstructured grids using multi-dimensional upwind schemes. PhD Thesis, Technische Universitet Delft 1998.
20. Abgrall R, Mezine M. Construction of 2^{nd}-order accurate monotone and stable rds for steady flow problems. *J. Comput. Physics* 2004; **195**:474–507.
21. Ricchiuto M, Villedieu N, Abgrall R, Deconinck H. On uniformly high-order accurate residual distribution schemes for advectiondiffusion. *Journal of Computational and Applied Mathematics* 2008; **215**(2):547 – 556, doi:http://dx.doi.org/10.1016/j.cam.2006.03.059. URL http://www.sciencedirect.com/science/article/pii/S0377042706007667, proceedings of the Third International Conference on Advanced Computational Methods in Engineering (ACOMEN 2005).
22. Sermeus K. Multi-dimensional upwind discretization and application to compressible flows. PhD Thesis, Université Libre de Bruxelles 2013.
23. Mazaheri A, Nishikawa H. Very efficient high-order hyperbolic schemes for time-dependent advection–diffusion problems: Third-, fourth-, and sixth-order. *Computers & Fluids* 2014; **102**:131–147.
24. Mazaheri A, Nishikawa H. High-order shock-capturing hyperbolic residual–distribution schemes on irregular triangular grids. *Computers & Fluids* 2016; **131**:131–147, doi:10.1016/j.compfluid.2016.03.012.

25. Larat A. Conception et analyse de schémas d'ordre très élevé distribuant le résidu : application à la mécanique des fluides. PhD Thesis, Université de Bordeaux I 2009.
26. Abgrall R, De Santis D, Ricchiuto M. High-order preserving residual distribution schemes for advection-diffusion scalar problems on arbitrary grids. *SIAM Journal Scientific Computing* 2014; **36**(3):A955–A983.
27. Abgrall R, Santis DD. Linear and non-linear high order accurate residual distribution schemes for the discretization of the steady compressible Navier–Stokes equations. *J. Comput. Physics* 2015; **283**:329 – 359, doi:https://doi.org/10.1016/j.jcp.2014.11.031. URL http://www.sciencedirect.com/science/article/pii/S0021999114007931.
28. Lani A, Deconick H. Conservative residual distribution method for hypersonic flows in thermochemical nonequilibrium. *Proceedings of the* 47^{th} *AIAA Aerospace Science Meeting and Exhibit*, AIAA: Orlando(FL), 2009.
29. Garicano-Mena, J, Lani, A, Degrez, G and Deconinck, H. A symmetrizing variables formulation for hypersonic thermo-chemical non-equilibrium flow, with application to residual distribution schemes. *V European Conference on Computational Fluid Dynamics*, 2010.
30. A Lani, J Garicano-Mena, and H Deconinck. A Residual Distribution Method for Symmetrized Systems in Thermochemical Nonequilibrium. AIAA 2011-3546, 20^{th} AIAA Computational Fluid Dynamics Conference, Honolulu, Hawaii, 2011.
31. Garicano-Mena J, Lani A, Deconinck H. An energy-dissipative remedy against carbuncle: Application to hypersonic flows around blunt bodies. *Computers and Fluids* 2016; **133**:43 – 54, doi:http://dx.doi.org/10.1016/j.compfluid.2016.03.028. URL http://www.sciencedirect.com/science/article/pii/S0045793016300858.
32. Garicano-Mena J, Lani A, Degrez G. An entropy-variables-based formulation of residual distribution schemes for non-equilibrium flows. *J. Comput. Physics* – 2018; **–**:682–702.
33. Paciorri R, Bonfiglioli A. A shock-fitting technique for 2D unstructured grids. *Computers and Fluids* 2009; **38**:715–726.
34. Bonfiglioli A, Grottadaurea M, Paciorri R, Sabetta F. An unstructured, three-dimensional, shock-fitting solver for hypersonic flows. *Computers & Fluids* 2013; **73**:162–174.
35. Pepe R, Bonfiglioli A, D'Angola A, Colonna G, Paciorri R. An unstructured shock-fitting solver for hypersonic plasma flows in chemical non-equilibrium. *Computer Physics Communications* 2015; **196**:179–193, doi:10.1016/j.cpc.2015.06.005.
36. Lani A, De Amicis V. SF: An open source object-oriented platform for unstructured shock-fitting methods. *Shock Fitting. Shock Wave and High Pressure Phenomena, edited by M. Onofri M. and R. Paciorri*, 2017, doi:10.1007/978-3-319-68427-7_4.
37. Anderson J. *Hypersonic and high temperature gas dynamics,* 2^{nd}*Ed.* AIAA Textbooks Series, American Institute of Aeronautics and Astronautics, 2006.
38. Deconinck H, Roe P, Struijs R. A multidimensional generalization of Roe's flux difference splitter for the Euler equations. *Computers and Fluids* 1993; **22**(2-3):215–222.
39. Struijs R, Deconinck H, Roe P. Fluctuation splitting for multidimensional convection problems: an alternative to finite volume and finite element methods. *LS 1990-04*, VKI 1990.
40. van der Weide E, Deconinck H, Issman E, Degrez G. A parallel, implicit. multi-dimensional upwind, residual distribution method for the Navier-Stokes equations on unstructured grids. *Computational Mechanics* 1999; **23**(2):199–208.
41. Villedieu N, Quintino T, Ricchiuto M, Deconinck H. Third order residual distribution schemes for the Navier–Stokes equations. *J. Comput. Physics* 2011; **230**(11):4301–4315, doi:http://dx.doi.org/10.1016/j.jcp.2010.12.026. URL http://www.sciencedirect.com/science/article/pii/S002199911000700X, special issue High Order Methods for CFD Problems.
42. Dobeš J, Ricchiuto M, Abgrall R, Deconinck H. On hybrid residual distribution-Galerkin discretizations for steady and time dependent viscous laminar flows. *Computer Methods in Applied Mechanics and Engineering* 2015; **283**:1336–1356.
43. Garicano-Mena J. On the computation of heat flux in hypersonic flows using residual distribution schemes. PhD Thesis, Université Libre de Bruxelles 2014.
44. Roe P. Linear advection schemes on triangular meshes. *Coa*, Cranfield Institute of Technology 1987.
45. van der Weide E, Deconinck H. Positive matrix distribution schemes for hyperbolic systems, with applications to the Euler equations. *Proceedings of the* 3^{rd} *European CFD conference*, Paris, 1996; 747–753.
46. Csìk A, Ricchiuto M, Deconinck H. Conservative formulation of the multidimensional upwind residual distribution schemes for general nonlinear conservation laws. *J. Comput. Physics* 2002; **179**(1):286–312.
47. Ricchiuto M. Construction and analysis of compact residual distribution discretizations for conservation laws on unstructured meshes. PhD Thesis, Université Libre de Bruxelles 2005.

48. Garicano-Mena J, Pepe R, Lani A, Deconinck H. Assessment of heat flux prediction capabilities of residual distribution method: Application to atmospheric entry problems. *Communications in Computational Physics* 3 2015; **17**:682–702, doi:10.4208/cicp.070414.211114a. URL http://journals.cambridge.org/article_S1815240615000146.
49. Dobeš J, Deconinck H. Second order blended multidimensional upwind residual distribution scheme for steady and unsteady computations. *Journal of Computational and Applied Mathematics* 2008; **215**(2):378 – 389, doi:http://dx.doi.org/10.1016/j.cam.2006.03.046. URL http://www.sciencedirect.com/science/article/pii/S0377042706007485, proceedings of the Third International Conference on Advanced Computational Methods in Engineering (ACOMEN 2005). Proceedings of the Third International Conference on Advanced Computational Methods in Engineering (ACOMEN 2005).
50. Lani, A, Panesi, M and Deconinck, H. Conservative residual distribution method for viscous double cone flows in thermochemical nonequilibrium. *Communications in Computational Physics* 2013; **13**:479–501.
51. Carette J. Adaptive Unstructured Mesh Algorithms and SUPG Finite Element Method for Compressible High Reynolds Number Flows. PhD Thesis, Université Libre de Bruxelles 1997.
52. Carette J, Deconinck H, Paillere H, Roe PL. Multidimensional upwinding: Its relation to finite elements. *International Journal for Numerical Methods in Fluids* ; **20**(89):935–955, doi:10.1002/fld.1650200815. URL https://onlinelibrary.wiley.com/doi/abs/10.1002/fld.1650200815.
53. Garicano-Mena, J, Lani, A, Degrez, G and Deconinck, H. Residual distribution schemes for the computation of hypersonic flows with strong bow shock waves: enforcing total enthalpy conservation. *VI European Conference on Computational Fluid Dynamics*, 2014.
54. Kirk BS, Carey GF, Stogner RH, Oliver T, Bauman PT. Recent advancements in fully implicit numerical methods for hypersonic reacting flows. *Proceedings of the* 21^{st} *AIAA Computational Fluid Dynamics Conference*, AIAA: San Diego, CA, 2013.
55. White F. *Viscous Flow,* 3^{rd} *Ed*. McGraw-Hill Science/Engineering/Math, 2005.
56. Lax P. Weak solutions of nonlinear hyperbolic equations and their numerical computation. *Communications on Pure and Applied Mathematics* 1954; **7**(1):159–193, doi:10.1002/cpa.3160070112. URL http://dx.doi.org/10.1002/cpa.3160070112.
57. Rusanov V. The calculation of the interaction of non-stationary shock waves and obstacles. *USSR Computational Mathematics and Mathematical Physics* 1962; **1**(2):304–320, doi:http://dx.doi.org/10.1016/0041-5553(62)90062-9. URL http://www.sciencedirect.com/science/article/pii/0041555362900629.
58. J Garicano-Mena, R Pepe, A Lani and H Deconinck. Assessment of Residual Distribution Method Heat Flux Prediction Capabilities: Application to Atmospheric Entry Problems. AIAA 2014-1391, 52^{nd} AIAA Aerospace Sciences Meeting, Washington(DC), 2014.
59. Koppenwallner G. Fundamentals of hypersonics: aerodynamics and heat transfer. *LS 1984-01*, VKI 1984.
60. Ko DRS, Kubota T. A second-order weak interaction expansion for moderately hypersonic flow past a flat plate. *AIAA Journal* 1967; **5**(10):1915–1917.
61. Carter J. Numerical solutions of the Navier-Stokes equations for the supersonic laminar flow over a two-dimensional compression corner. *Technical Report TR R-385*, NASA 1972.
62. Garicano-Mena, J and Lani, A and Sermeus, K and and Deconinck, H. An effective treatment of numerical shock wave instabilities with residual distribution schemes: Application to hypersonic nonequilibrium flows around blunt bodies. 7^{th} *European Symposium on Aerothermodynamics for Space Vehicles*, Brugge, Belgium, 2011.
63. Gnoffo PA. Updates to multi-dimensional flux reconstruction for hypersonic simulations on tetrahedral grids. *Proceedings of the* 48^{th} *AIAA Aerospace Science Meeting and Exhibit*, AIAA: Orlando(FL), 2010.
64. Abgrall R. Residual distribution schemes: Current status and future trends. *Computers & Fluids* 2006; **35**(7):641 – 669, doi:https://doi.org/10.1016/j.compfluid.2005.01.007. URL http://www.sciencedirect.com/science/article/pii/S0045793005001738, special Issue Dedicated to Professor Stanley G. Rubin on the Occasion of his 65th Birthday.
65. Deconinck H, Ricchiuto M, Sermeus K. Introduction to residual distribution schemes and stabilized finite elements. *LS 2003-05*, VKI 2003.
66. Lani A, Villedieu N, Bensassi K, Kapa L, Vymazal M, Yalim MS, Panesi M. COOLFluiD: an open computational platform for multi-physics simulation and research. *AIAA 2013-2589*, 21th AIAA CFD Conference: San Diego (CA), 2013.
67. Saad Y. *Iterative methods for sparse linear systems: Second edition*. SIAM, 2003.
68. S Balay JB. Petsc users manual. *Technical Report ANL-95/11 - Revision 3.4*, Argonne National Laboratory 2013.

DOI: 10.1002/fld